# The Lanthanide Tetrad Effect as an Exploration Tool for Granite-Related Rare Metal Ore Systems: Examples from the Iberian Variscan Belt

Ivo M. Martins, António Mateus, Michel Cathelineau, Marie Christine Boiron, Isabel Ribeiro da Costa, Ícaro Dias da Silva, Miguel Gaspar

# The lanthanide tetrad effect as an exploration tool for granite-related rare metal ore systems: examples from Iberian Variscides

**Ivo Martins [1,2,*], António Mateus [1,2], Michel Cathelineau [3], Marie Christine Boiron [3], Isabel Ribeiro da Costa [1], Ícaro Dias da Silva [1,2] and Miguel Gaspar [1]**

1- Departamento de Geologia, Faculdade de Ciências da Universidade de Lisboa, Ed. C6, Piso 4, Campo Grande, 1749-016 Lisboa, Portugal; amateus@fc.ul.pt (A.M.); imscosta@fc.ul.pt (I.R.C.); lmgaspar@fc.ul.pt (M.G.); ipicaparopo@gmail.com (I.D.S.)
2- Instituto Dom Luiz (IDL), Faculdade de Ciências da Universidade de Lisboa, Ed. C1, Piso 1, Campo Grande, 1749-016 Lisboa, Portugal
3- Université de Lorraine, CNRS, CREGU, GeoRessources, F-54000 Nancy, France; michel.cathelineau@univ-lorraine.fr (M.C.); marie-christine.boiron@univ-lorraine.fr (M.C.B.)
*Correspondence: ijmartins@fc.ul.pt (I.M.)

Abstract: Granite differentiation and related magmatic-hydrothermal ore-forming processes can be traced by elemental content ratios such as Nb/Ta, K/Rb, Y/Ho, Sr/Eu, Eu/Eu*, Zr/Hf and Rb/Sr. The lanthanide tetrad effect (TE1,3) is also a useful whole-rock geochemical fingerprint of granite differentiation. Its application as an exploration vector for granite-related mineralization in the Central Iberian Zone (CIZ) is assessed in this work by examining the TE1,3 variations along with different elemental ratios, and with the concentrations of rare-metals contents and fluxing elements. The multi-elemental whole-rock geochemical characterization of the Cambri-an-Ordovician and Carboniferous-Permian main granite plutons and late aplite-pegmatite dykes exposed across the Segura-Panasqueira Sn-W-Li belt show that increasing TE1,3 values (up to 1.4) co-vary with magmatic differentiation and metal-enrichment, and that the Carboniferous-Permian granite rocks are more differentiated, and metal specialized. The Argemela Li-Sn-bearing Rare Metal Granite (RMG) and the Segura Li-phosphate-bearing aplite-pegmatite dykes deviate from this geochemical trend, displaying TE1,3 <1.1, but high P2O5 contents. The results obtained suggest that mineralized rocks related to Peraluminous-High-Phosphorous Li-Sn granite systems are typified by TE1,3 <1.1, whereas those associated with Peraluminous-High-Phosphorous Sn-W-Li (lepidolite) and Peraluminous-Low-Phosphorous Sn-Ta-Nb granite systems display TE1,3 >1.1, reaching values as high as 1.4 and 2.1, respectively.
Keywords: CIZ magmatism; granite differentiation; granite-related ore systems; lanthanide tetrad effect; mineral exploration

## 1. Introduction

Current technological evolution and energy transition policies amplify the de-pendence of a large number of metals, many of them with low recycling rates. This generates additional pressure on mineral exploration endeavors to search new primary resources for these

strategic metals, which are often associated with highly evolved muscovite-bearing peraluminous granites [1-4].

Granite-related ore systems include mostly: (i) quartz lodes, breccia pipes and skarns enriched in W-Sn-F(-P)-bearing mineral assemblages, and (ii) rare-metal granites and pegmatite-hosted mineral assemblages enriched in Li-Cs-Be-Ta(-P) and/or Nb-Y-F(-Sn) [e.g., 1,5]. There are numerous examples of granite-related ore systems with different mineralization styles coexisting in Europe, forming a Sn-W-Li world-class province of Paleozoic age [6-14]. The Segura-Panasqueira area, sited in the Central Iberian Zone (CIZ – a geotectonic unit of Iberian Variscides), is part of the well-defined Late Palaeozoic granite-related European metallogenic belt, wherein voluminous peraluminous granite suites with distinct degrees of differentiation are associated with varied styles of W, Sn and Li ore systems.

The granite differentiation and related magmatic-hydrothermal ore-forming processes can be traced by elemental content ratios such as K/Rb, Sr/Eu, Y/Ho, Rb/Sr, Nb/Ta and Zr/Hf [4,15-19]. The lanthanide tetrad effect is also a useful whole-rock geochemical marker of magmatic evolution and magmatic-hydrothermal transition, corresponding to a specific form of rare earth element (REE) fractionation, evidenced by the subdivision of the chondrite-normalized REE patterns into four curved segments that are called tetrads [17,20]. This REE fractionation is commonly observed in highly evolved felsic magmatic rocks and related metasomatic rocks, but also in precipitates from hydrothermal fluids, accessory minerals and melt inclusions [15,17,21-26]. There are two types of tetrad effects with the curved segments being either convex or concave (M-type or W-type, respectively). These two types are derived from each other, being that the M-type tetrad effect is characteristic of highly evolved granite samples from which is extracted a W-type REE pattern representing a coexisting fluid [17,20,27,28]. The existence and geochemical significance of the degree of tetrad effect (TE1,3) can be quantified by determining the respective deviation of the first and third tetrad of a chondrite-normalized REE pattern from a theoretical tetrad effect-free pattern. The tetrad effect is significant when TE1,3 >1.1 [17].

In this work the application of the TE1,3 as an exploration vector for granite-related mineralization is assessed by examining the TE1,3 variations along with other geochemical parameters, the contents of rare metals (Sn, W, Nb, Ta, Li) and fluxing elements. For that purpose, new whole-rock multi-elemental geochemical data of the main (composite) plutons and dykes exposed across the Segura-Panasqueira area are reported, supporting a comprehensive geochemical characterization of: (i) granite and granodiorite rocks that represent different regional magmatic pulses; and (ii) late Rare Metal Granite (RMG), aplite-pegmatite dykes and greisen rocks from Argemela, Segura and Panasqueira representing the W, Sn and Li granite-related ore systems. The degrees of differentiation and mineralization potential, as well as the applicability of the TE1,3 as an exploration tool for granite-related ore systems will be discussed, along with the geochemical composition of granite rocks from other sectors of the Variscan orogeny.

## 2. Geological Setting

The Segura-Panasqueira area is located in the Central Iberian Zone (CIZ), which forms the central part of the Iberian segment of the Variscan orogenic belt (Figure 1a). The tectonic evolution of the Variscan belt is controlled by the Gondwana-Laurasia collision and subsequent closure of the Rheic Ocean (Middle-Devonian to Middle-Carboniferous) followed

by late (post-thickening) lithospheric rebound and stress relieving (Mid-dle-Carboniferous to Permian) [29-33].

Three main deformation phases (D1, D2 and D3) have been distinguished in this domain of the Variscan orogenic belt [29,30,34-37]. The D1 and D2 [359-336 and 337-316 Ma, respectively; 32,38-40] deformation phases reflect the maximum of Variscan crustal shortening during which folds of large amplitude were generated: these folds display variable geometry and orientation depending on the orogenic sector, presenting a NW-SE preferred strike with sub-vertical axial planes [30,41].

Concurrently with D1 folding and often reflecting thermo-mechanic contrasts generated during heterogeneous strain accommodation, several regional ductile syn-D1 shear zones were also developed. After the tectonic emplacement of the allochthonous piles typifying the NW Iberia (D2), intra-continental strike-slip sinistral and dextral sub-vertical semi-brittle shear zones were formed during D3 [44,45], together with folds displaying sub-vertical axial plane and sub-horizontal axis [41,46]. These sub-vertical shear zones, locally reactivating previous syn-D1 shears, are quite often confined to the edges of voluminous granite batholiths [35,47-53]. The spatial distribution of shear zones and folds allow to infer NE-SW maximum compression trajectories [54], not significantly deviating from the stress configuration characterizing the previous deformation phases. The D3 [315-306 Ma; 36,40,47] deformation phase took place mostly after the climax of crustal thickening during which large volumes of crustal melting were produced [36,46,55]. Late- to post- D3 [310-270 Ma; 54,56] conjugate strike-slip fault systems running NNE-SSW (left-lateral) and NNW-SSE (right-lateral) were further generated in brittle deformation conditions, locally reactivating syn-D3 (and syn-D1) shear zones [e.g., 34-36,41].

The Beira-Baixa region, where the Segura-Panasqueira area is situated, comprises voluminous granite bodies hosted in a folded siliciclastic metasedimentary succession that was recrystallized under P-T conditions of greenschist metamorphic facies. The metasedimentary succession corresponds to the Dúrico-Beirão Supergroup [e.g., 57-61], which includes the Douro Group (Lower- to Middle-Cambrian) and the Beiras Group (Neoproterozoic to Lower-Cambrian). Granitoid rocks cropping out in CIZ show a wide range of facies and compositions [37], resulting from the partial melting of various protoliths, mainly at the mid-lower crust transition, such as metapelites, meta-greywackes and metavolcanic rocks. In some cases, contributions from lower crustal granulites were also proposed [47,62]. Following the classification criteria based on the age relationship between the emplacement of these rocks and D3, granites are usually classified into 4 main subgroups [e.g., 47,63-66]:

(i) Syn-D3 (ca. 320 to 310 Ma) - essentially two-mica granites, strongly peralu-minous, with aluminium-potassic affinity, representing the crystallization of magmas derived from the partial melting of metapelites;

(ii) Late-D3 (ca. 310 to 305 Ma) - mainly moderately peraluminous and aluminium-potassium biotitic monzogranites/granodiorites with aluminium-potassic affinity, resulting from the crystallization of magmas generated from partial melting of metagreywacke and/or felsic meta-igneous materials;

(iii) Late- to Post-D3 (ca. 300 Ma) - basically peraluminous leucogranite of two micas with high aluminium-potassic affinity;

(iv) Post-D3 (ca. 296 to 290 Ma) - compositionally evolved granitoids with iron-potassic sub-alkaline affinity integrating products derived from partial melting of lower crust rocks.

The geological evolution of Iberia during Paleozoic times conditioned the spatial distribution of granitic bodies along certain crustal alignments in the CIZ [e.g., 41,47]. The generation of prevalent melts was roughly contemporary of D3 folding, favoring the emplacement of granite rocks across the core of major D3 anticlines [e.g., 37]. Thermo-mechanic contrasts developed during the cooling of these granites and their country rocks, under a strong stress regime, led to the nucleation and propagation of syn-D3 shear zones, further representing the preferred locus for strain accommodation. Locally, these tectonic discontinuities played an important role as conduits of melts generated and emplaced in late-, late- to post- and post-D3 times [e.g., 41]. The relative intensity of regional stress field and local interferences with the stress fields related to the emplacement/cooling of granite bodies allowed the development of several subsidiary structures which might have reactivate pre-existing mechanical discontinuities in country rocks [e.g., 67-70].

The known epigenetic mineralized systems in CIZ are closely related to the aforementioned granite suites, at least spatially (Figure 1b). This highlights the im-portance/influence of the Variscan orogeny in the onset and further support of different metallogenic processes over millions of years, leading to the formation of distinct and spatially coexistent ore systems [e.g., 66]. The spatial distribution of Sn, W and Li occurrences follows the dispersion of outcropping or sub-superficial granite bodies, the latter often evidenced by contact metamorphic aureoles of variable extension and distinct mineral blastesis. Despite this evident spatial relationship, the progression of Sn, W and Li mineralizing systems is not exclusively related to the magmatic activity since the ore-forming processes are multiphasic and long-lived, involving phenomena related to late magmatic stages (emplacement and early cooling phases of highly differentiated granite melts) followed by hydrothermal activity that could have remained strong enough for several millions of years [e.g., 13,43,66]. Therefore, the gran-ite-metasedimentary binary is not only relevant in the generation of some types of melts but also in the constraints imposed to the production of hydrothermal fluids (volume and composition) involved in the ore-forming processes [e.g., 71].

The location of the main W, Sn and Li ore systems is largely controlled by inherited structures (such as shear zones and other structural lithospheric weaknesses) that were also determinant in the emplacement of post-tectonic granites [72], both occurring along granite-metasediment or diachronic granite contacts [73]. The mineralization centers may occur in endo- and exo-contact domains, contributing to the development of geochemical zoned patterns often described by the following succession: Sn-Li-bearing pegmatites and/or Sn-Li-bearing quartz veins within endo-contact domains; Sn-W quartz veins scattered all over the endo/exo-contact transition but extending preferentially to exo-contact domains; and W-quartz veins within exo-contact domains [74].

The Segura-Panasqueira area, which is the focus of this study, is characterized by a prevailing siliciclastic (shale-greywacke) metasedimentary succession belonging to the Beiras Group that host several voluminous granite bodies. Numerous mineral occurrences were recognized in this area, indicating a significant metallogenic potential (Figure 1b). Three main groups of granitoid rocks are known in the Segura-Panasqueira area (Figure 2), which document two (relatively short) time events of magmatic activity favorable to the generation and emplacement of felsic magmas [75- 85]. The first group is composed of (i) two mica granitoids with restites, (ii) biotitic quartz-diorites and granodiorites, and (iii) non-porphyroid granites and granodiorites, representing a Cambrian-Ordovician magmatic event spreading for about 20 Ma (from ca. 490 Ma to 470 Ma). The two remaining groups, syn- to late-D3 and late- to post-D3, typify a Carboniferous-Permian (Variscan) magmatic event that extends

for approximately 30 Ma (from ca. 320 Ma to 290 Ma). The syn-D3 group is composed of (i) porphyroid granites and granodiorites, and (ii) undifferentiated two-mica granites. The late- to post-D3 group comprises (i) two-mica granites, (ii) monzonitic granites with sparse feldspar megacrystals, (iii) porphyroid monzonitic granites, and (iv) biotitic, usually porphyroid, granites. This last group also includes the highly differentiated granite rocks that are key-references for granite-related ore systems, such as the Panasqueira granite, Li-Sn Argemela RMG and Li-Sn-bearing aplite-pegmatites dykes of Segura.

## 3. Materials and Methods

During 2019-2021, a sampling campaign was performed in the Segura-Panasqueira area to gather representative samples of the different granite suites and highly differentiated granitic pegmatite and aplite veins (Figure 2), aiming their multi-element whole-rock geochemical characterization. The sampling criteria used were: (i) to complement existing data for exposed rock types by collecting granite facies from sites where information gaps exist; (ii) to achieve a spatially representative sampling of different outcropping igneous facies; (iii) to sample, preferentially, along waterlines and non-covered river margins where the bedrock is usually well preserved; (iv) to gather samples from different mineralization types, aiming the identification of geochemical fingerprints imposed by hydrothermal processes.

A total of 75 samples were collected, as follows: (i) 51 of felsic igneous bodies; (ii) 18 of felsic igneous dykes; and (iii) 6 of greisen and epysienite rocks from the Panasqueira Mine area. Although most of the samples were collected from outcrops (58), critical drillings and mining works from Panasqueira and Argemela were also sampled (17). Samples considered crucial and representative of the different granite facies (poorly to highly differentiated) were selected, processed, and sent to internationally accredited laboratories for high precision whole-rock geochemistry analysis (49). Whole-rock major and trace element concentrations were obtained at Activation Laboratories, Ltd. (Ancaster, Ontario, Canada), using the geochemical analytical package 4E-research+ICPMS. Major oxide elements were analyzed by inducing coupled plasma optical emission spectrometry (ICP-OES). Trace and rare earth elements (REE) were obtained by inducing coupled plasma mass spectrometry (ICP-MS) and instrumental neutron activation analysis (INAA). In addition, F, B and FeO contents were measured with KOH-ion chromatography, Prompt gamma neutron activation analysis (PGNAA) and titration, respectively.

Detailed information regarding the analytical and control procedures can be found in the Actlabs website (www.actlabs.com). Afterwards, these samples were used as in-house standards for the remaining samples analyzed with X-ray fluorescence (XRF) at the Faculdade de Ciências da Universidade de Lisboa (Portugal). The accuracy-related errors in XRF measurements were ≤ 5% for major elements and better than 10% for the most widely used incompatible elements. Duplicate measurements of samples indicate also that reproducibility-related errors in XRF analyses were generally ≤ 5% for both major and trace elements.

## 4. Results

The whole-rock multi-element data of the main (composite) granite plutons and aplite-pegmatite dykes exposed across the Segura-Panasqueira area are listed in Table S1. Based on facies description and geochronology information from previous works (Table S1), besides observed field relationships, the sampled rocks represent two main regional magmatic pulses: Cambrian-Ordovician and Carboniferous-Permian (Variscan). The

Cambrian-Ordovician magmatic event is represented by the composite plutons of Ze-breira [80], Oledo-Idanha-a-Nova [82], Fundão [83, 85], Batão and Matos. The Variscan magmatic event is characterized by the Salvaterra do Extremo (Syn-D3?), Castelo Branco [Late-D3; 81], Segura [Late-D3; 84], Orca [Late-D3; 94], Penamacor-Monsanto [Late- to Post-D3; 95, 96], Capinha [Late- to Post-D3; 94], Atalaia [Late- to Post-D3; 94] and a porphyry intrusion near Zebreira (Late- to Post-D3?). It is worth noting that in all the cross-plots, intersection between the compositional fields of the two magmatic events is mainly due to the spreading of samples representing the less differentiated facies of the Castelo Branco pluton (CB-G2) and the more differentiated facies of the Zebreira, Ole-do-Idanha-a-Nova and Fundão plutons (G_ZEB#1 and G_ZEB#4; OIN-G3 and G4; FUN-G1 and FUN-G3). In addition, field observations suggest that these differentiated Cambrian-Ordovician facies are invariably younger than the less evolved ones, often showing crisscrossing relationships and textural fabric contrasts that point to significant differences in their emplacement timings. Therefore, to clarify whether they are being attributed to the correct magmatic event or if they correspond to late magmatic pulses of Variscan age, these differentiated facies were selected for U-Pb zircon dating as future work.

In geochemical data interpretation, the aplite-pegmatite dykes from Ole-do-Idanha-a-Nova, Orca and Penamacor-Monsanto, together with granite rocks related to Li-Sn and W-Sn ore systems from Argemela [97], Segura and Panasqueira [98], were examined separately. Since these rocks are highly differentiated and/or interacted with magmatic-hydrothermal processes, they should not be used in conventional diagrams of geochemical classification of granite rocks. Relatively to the rare earth elements, only the analyses with the lowest detection limits and complete REE patterns were considered. The degree of the tetrad effect was estimated by the methods of quantification proposed by Irber (1999) and Monecke (2002) (Table S.2 and Table S.3). Since the use of both methods yielded similar results, in this work we will present those of the TE1,3 [17] due to graphical simplification.

4.1. Major and minor elements

The majority of the Cambrian-Ordovician granitoid rocks are weakly peraluminous I-type (mean ASI value of 1.11), biotite/biotite>muscovite tonalite to granodiorite rocks (Figure 3). They present relatively moderate values of SiO2 (mean value of 68.19 wt%), total alkalis (mean Na2O+K2O value of 6.87 wt%) and FeOtotal/(FeOtotal+MgO) ratio (mean Fe* value of 0.66), with most samples plotting into the compositional fields of calcic to calc-alkalic series and magnesian granites (Figure 4-a and b). In turn, the Variscan magmatism event is mainly characterized by highly peraluminous S-type (median ASI value of 1.25), muscovite>biotite/biotite>muscovite monzogranite to granite rocks (Figure 3). Variscan granite rocks show relatively high values of SiO2 (median value of 72.71 wt%), total alkalis (median value of 8.12 wt%) and FeOtotal/(FeOtotal+MgO) ratio (median value of 0.79), plotting into the calc-alkalic to alkali-calcic series and magnesian to ferroan granites compositional fields (Figure 4-a and b). Regarding the degree of magmatic differentiation, the Cambrian-Ordovician granitoid suites range from diorite to normal granite compositions and display condensed differentiation trends in comparison with those characterizing Variscan granites. The latter are strongly differentiated rocks, as confirmed by their contents in Ba, Rb and Sr (Figure 4-c). The tectonic discrimination diagrams of Pearce et al. (1984) show that most of the Cambrian-Ordovician granitoid rocks plot in the compositional field of volcanic arc granites whereas the Variscan granites cluster in the syn-collisional granites field (Figure 5).

As previously mentioned, the compositional deviations of the Cambrian-Ordovician granitoids towards the Variscan magmatism composition are only related with the late facies of the Zebreira, Oledo-Idanha-a-Nova and Fundão plutons. These rocks are moderately peraluminous S-type (mean ASI value of 1.23), muscovite>biotite/biotite>muscovite monzogranite to granite rocks (Figure 3). They also present high SiO2 (mean value of 73.88 wt%), total alkalis (mean value of 8.34 wt%) and Fe* ratio (mean value of 0.82) values, plotting in the calc-alkalic to alkali-calcic series and magnesian to ferroan granites fields (Figure 4-a and b). Relatively to their tectonic settings and magmatic differentiation degree, these facies display compositional features of syn-collisional and strongly differentiated granites (Figure 4-c and Figure 5).

Considering the A-B classification diagram for felsic rocks of Debon and Lefort (1988), modified by Cuney (2014) and Romer and Pichavant (2020), it is possible to classify the highly differentiated rocks along the evolution path of the aluminium saturation index, during the processes of magmatic fractionation. This diagram is based on some minor minerals (e.g., Al-silicates, muscovite, topaz, cordierite, garnet, biotite, amphibole, py-roxene), and usually only the highly evolved rare-metal granites and aplite-pegmatite dykes deviate from the origin of the diagram (point of extreme fractional crystallization) to higher A values. The granite facies and aplite-pegmatite dykes of Argemela, Panasqueira, Segura, Oledo-Idanha-a-Nova, Orca and Penamacor-Monsanto, follow the typical S-type granites fractionation trend, falling mostly in the leucogranites field, near the RMG composition. The deviation from this general trend is essentially justified by the geochemical composition of the Panasqueira greisen, Argemela RMG and ap-lite-pegmatite dykes from Argemela and Segura that display variable A values, reflecting late magmatic-hydrothermal interactions and/or strongly peraluminous melt compositions able of stabilize muscovite, lepidolite, Li-Al-phosphates (montebrasite-amblygonite) and topaz (Figure 6).

4.2. Trace elements

The Upper Continental Crust-normalized (UCC, Rudnick and Gao, 2014) multielement patterns for the Cambrian-Ordovician and Variscan magmatic events (Figure 7-a and b) are mostly characterized by: positive anomalies in P, Li, B, Cs, Ta, and U; and negative anomalies in Ba, Zr, and Th, usually much more evident for samples representing the Variscan magmatic event. In addition, the Variscan granitoid facies display positive anomalies in Be and Sn and negative anomalies in F, Rb and Y. Regardless the type of anomalies, these two magmatic events show UCC-normalized patterns with signs of important enrichment in P, F, Be, Li, B, Rb, Cs, Ta, Sn, W and U, and depletion in Ba, Sr, Zr, Hf, Th and Y, always more significant in the Variscan granite facies. The highly differentiated granite facies and aplite-pegmatite dykes are mainly characterized by positive anomalies in P, Be, Li, Rb, Ta, Sn, Hf and U, and negative anomalies in F, B, Ba, Zr, Th and Y (Figure 7-c). In addition to the relative enrichments and depletions in the same elements observed for the granite facies from the Cambrian-Ordovician and Variscan magmatic events, the highly differentiated granite facies and aplite-pegmatite dykes also record higher enrichments in Nb. In general, all the elemental anomalies are more pronounced in the differentiated granite facies and aplite-pegmatite dykes, especially for the P, F, Be, Li, Ta and Sn enrichments.

4.3. Rare earth elements

Rare Earth Elements (REE) compositional data are summarized in Table S.2. The chondrite-normalized (CN, McDonough and Sun, 1995) patterns show that rocks representing the Cambrian-Ordovician and the Variscan magmatic events display wide REE concentration ranges (ΣREE = 10.41 to 171.95 ppm; ΣREE = 8.88 to 194.60 ppm, respectively) but present similar chondrite-normalized patterns (Figure 8-a and b). Both patterns are negatively sloped, showing Light Rare Earth Elements (LREE) enrichments relatively to the Heavy Rare Earth Elements (HREE) (La/YbCN = 1.68 to 23.36; La/YbCN = 1.79 to 25.61, respectively), with different degrees of HREE fractionation (Dy/YbCN = 0.80 to 2.62; Dy/YbCN = 1.28 to 4.06, respectively) and negative Eu anomalies (Eu/Eu* = 0.31 to 1.04; Eu/Eu* = 0.05 to 0.64, respectively) that tend to be more pronounced in samples from the Variscan granite suites. The similarities in REE fractionation for samples from Cambrian-Ordovician and Variscan suites, with slightly differences in the HREE, explain the comparable degrees of tetrad effect, with the Variscan granites recording a tendency for slightly higher values (TE1,3 = 0.95 to 1.20 for the Cambrian-Ordovician suite; TE1,3 = 0.99 to 1.30 for the Variscan suite). Considering the chondrite-normalized patterns of the highly differentiated granite facies and aplite-pegmatite dykes, it is possible to distinguish two main groups (Figure 8-c). The first group includes samples representing the Panasqueira Granite facies, the Segura Li-Sn lepidolite-bearing aplites, Penamacor-Monsanto pegmatite, Orca pegmatite and Oledo-Idanha-a-Nova aplite-pegmatite dykes and is typified by M-type (convex) chondrite-normalized patterns. These felsic rocks have a wide range of REE contents (ΣREE = 0.64 to 83.78 ppm), negatively sloped chondrite-normalized patterns (La/YbCN = 1.47 to 12.52), slightly flat HREE (Dy/YbCN = 0.31 to 1.87) and pronounced negative Eu anomalies (Eu/Eu* = 0.08 to 0.76), being characterized by significant degrees of tetrad effect (TE1,3 = 1.01 to 1.38). The second group comprises samples of the Panasqueira Greisen, Rare Metal Granite and aplite-pegmatite dykes from Argemela and the Li-phosphates-bearing pegmatite dykes from Segura, being mostly characterized by W-type (concave) chondrite-normalized patterns. These highly differentiated rocks have low contents of REE (ΣREE = 0.46 to 4.27 ppm), positively to negatively sloped chon-drite-normalized patterns (La/YbCN = 0.40 to 24.00), low HREE fractionation (Dy/YbCN = 0.35 to 1.53), moderate negative to strongly positive Eu anomalies (Eu/Eu* = 0.41 to 1.80) and extremely low TE1,3 values (0.71 to 1.09), consistently documenting the absence of a tetrad effect [17]. The implication of such division into two different geochemical groups and its relevance for the exploration of W-Sn-Li granite-related ore deposits will be discussed in the following section.

## 5. Discussion

### 5.1. Granite differentiation and metal specialization: correlation with TE1,3

To assess the usefulness of the TE1,3 as a marker of granite differentiation and as an exploration tool for granite-related rare metal ore systems, it is first necessary to evaluate the degrees of differentiation and metal specialization of the granitoid suites considered in this work. For that purpose, (i) the element ratios Nb/Ta, K/Rb, Y/Ho, Sr/Eu, Eu/Eu*, Zr/Hf and Rb/Sr were considered as geochemical granite differentiation markers; (ii) the values of Nb/Ta <5, K/Rb <150, Y/Ho ≠28, Sr/Eu > 200 and Eu/Eu* <0.1 were used as indicators of significant magmatic-hydrothermal processes [4,17]; and (iii) representative compositions of granite suites with different degrees of differentiation and metal-enrichments from other sectors of the Variscan orogeny (Table S.3) were also plotted to ascertain the fundamental geochemical trends built on a wide and robust dataset. The latter granite suites include the following reference cases: the Cambrian-Ordovician Beira-Extremadura Batolith [108]; the

Armorican Massif, Erzgebirge-Fichtelgebirge and Cornwall Variscan granites [4 and references therein]; the Variscan Penouta Sn-Ta-Nb RMG [109]; and several other Iberian Massif Variscan granites [4 and references therein, 110].

Granite facies with lower Nb/Ta ratios also display tendency to lower values of K/Rb, Eu/Eu* and Zr/Hf, and higher values of Y/Ho, Sr/Eu and Rb/Sr (Figure 9), showing a clear correlation between the different element ratios. Moreover, a good compositional similarity is observed between the studied samples and the published data for similar rocks from other Variscan crustal segments (Figure 9). Whereas most of the weakly peraluminous Cambrian-Ordovician rocks are the less evolved facies, the highly peraluminous Variscan granite facies and late aplite-pegmatite dykes are strongly differentiated and significantly affected by magmatic-hydrothermal processes (Figure 9-a to d and f). The most evolved rocks are the granite facies of Segura, Salvaterra do Extremo, Penamacor-Monsanto, Panasqueira, Argemela and Penouta and the aplite-pegmatite dykes from Oledo-Idanha-a-Nova, Segura, Penamacor-Monsanto and Argemela. Additionally, Nb/Ta vs. Zr/Hf [18] and Rb/Sr vs. Sn [19] can also be considered as geochemical indicators of the fertility of granitic rocks, separating barren granites from Sn-W(-U)-specialized granites and (Ta-Cs-Li-Nb-Be-Sn-W)-enriched/related granites. The Cambrian-Ordovician magmatism is essentially characterized by barren granites, and the Variscan magmatism tend to be more fertile, especially for Sn-W-(U) granite-related ore deposits. The more evolved rocks and most affected by late magmatic-hydrothermal fluids display specialized features of Ta-Cs-Li-Nb-Be-Sn-W granite-related ore systems. Among the samples that are part of the latter suite, the granite facies of Argemela and Penouta as well as the ap-lite-pegmatite dykes of Argemela and Segura are the most specialized (Figure 9-e and f). This granite differentiation followed by significant compositional modifications ascribed to magmatic-hydrothermal processes led to a progressive enrichment in granitophile elements, such as Sn, Li, Nb, Ta, Be and Cs (Figure 10-a to f).

The increase of TE1,3 values tend to co-vary with magmatic differentiation and metal-enrichment, as documented by the contrast between the poorly differentiated Cambrian-Ordovician granite suites with the lowest TE1,3 values (up to 1.2) and the Variscan granite facies showing a gradually higher TE1,3 (up to 2.1 - Penouta RMG) (Figure 10-g). Although the Li-phosphate-bearing Argemela RMG and aplite-pegmatite dykes from Argemela and Segura present the higher differentiation degrees and metal enrichments, they deviate from this geochemical trend having no evidence of tetrad effect (TE1,3 <1.1). Moreover, it is worthy to highlight that, based on the TE1,3, there is a sepa-ration between these Li-phosphate-bearing dykes and the lepidolite-bearing aplites from Segura, which follow the general trend. As suggested by Irber (1999), the development of a lanthanide tetrad effect (M-type) with pronounced negative Eu* in highly evolved granitic rocks implies the removal of a respective mirroring REE-pattern (W-type) with positive Eu*, corresponding to a coexisting high-temperature aqueous fluid. Therefore, although most of the granite facies are characterized by REE signatures of silicate melts with gradually higher degrees of differentiation, the Argemela RMG and the Li-phosphates-bearing aplite-pegmatite dykes from Argemela and Segura show com-positional signatures comparable with those expected for high-temperature aqueous fluids, as indicated by the absence of tetrad effect (TE1,3 <1.1) and by the tendency of Eu* anomalies to be positive (Figure 9-d).

5.2. The TE1,3 as an exploration vector for granite-related ore systems

In many granite systems, differentiation improvements lead to gradual enrichments of fluxing components ($H_2O$, P, F, B) in the melt that, in extreme fractionation degrees, could be complemented by a segregation of a $H_2O$-saturated melt and a high-temperature aqueous fluid [97, 111-113]. The crystallization of highly evolved silicate melts co-existing with aqueous high-temperature fluids results in important changes of the geochemical behavior of elements. In such circumstances the element fractionation is no longer exclusively controlled by the ionic radius and charge, and rare metals partition will preferentially go to the exsolved fluid phase [4, 15, 17]. Thus, to understand how the opposite signatures of REE fractionation in different granite-related ore systems (Li-Sn, W-Sn and Sn-Ta-Nb) are influenced by these magmatic-hydrothermal processes and relative predominance of P, F and B, it is important to observe their correlation with TE1,3 (Figure 11). On this basis, three main geochemical trends can be distinguished, which interpretation must consider the nature of accessory minerals in granite facies that are the main REE carriers (e.g., apatite, monazite, zircon, xenotime, fluorite, and garnet) and inherit the TE1,3 signature of the melt or of the high-temperature aqueous fluid from which they crystallize [17].

The first trend depicts magmatic-hydrothermal systems dominated by P and F (P+F±B, P>F) analogous to those typified by the Li-Sn Argemela RMG and Li-phosphate-bearing aplite-pegmatites from Segura. In these Peraluminous-High-Phosphorus (PHP) systems, with high contents of $P_2O_5$ and Li (up to 4.76 wt% and 1.27 wt%, respectively) and low contents of CaO (lower than 0.85 wt%), the main phosphate phases belong to the amblygonite-montebrasite series. The strongly negative correlation between $P_2O_5$ and TE1,3 suggest that these phosphate phases incorporate the REE signature of the late high-temperature aqueous fluid from which they precipitated. The second geochemical trend describes Peraluminous-High-Phosphorus magmatic-hydrothermal systems dominated by F and P (F+P±B, F>P), comparable to those represented by the W-Sn Panasqueira Granite facies and the Li-Sn, lepidolite-bearing aplites from Segura. These highly evolved rocks have slightly higher contents in F (up to 2300 ppm) and CaO (up to 1.7 wt%) and lower contents in $P_2O_5$ (below 1.94 wt%), ordinarily expressed as fluor-apatite often coupled with Li-bearing micas. For these magmatic-hydrothermal systems, the typical high TE1,3 values match those of highly evolved silicate melts interacting with aqueous fluids (up to 1.4), and the fluor-apatite should act as the main REE mineral carrier, as suggested by the positive co-variation of $P_2O_5$ and F with TE1,3. The third compositional trend describes Peraluminous-Low-Phosphorus (PLP) magmatic-hydrothermal systems dominated by F and B (F+B±P, F>B), as those illustrated by the topaz-, tourmaline- and garnet-bearing granites related to Sn-Ta-Nb ore systems like the cases of Penouta RMG and granite facies of Erzgebirge-Fichtelgebirge and of Penamacor-Monsanto. These strongly differentiated rocks are characterized by the higher TE1,3 values (up to 2.1), probably reflecting and inherited feature from the highly evolved silicate melt coexisting with a late magmatic-hydrothermal fluid; topaz and/or other F-rich phase are the prevalent mineral proxy, as evidenced by the co-variation between F contents and TE1,3 values.

In summary, the degree of the lanthanide tetrad effect is a useful whole-rock geo-chemical fingerprint of granite differentiation for silicate magmatic-hydrothermal systems dominated by F and B and with strong granitic magma REE signatures. In such cases the TE1,3 co-varies with increasing granite differentiation. For the late magmatic-hydrothermal systems dominated by P and F, represented by Li-phosphate-bearing rare-metal granites and aplite-pegmatites dykes, the negative correlation between the high degrees of differentiation and

the low values of the degree of the tetrad effect (TE1,3 <1.1) suggest that these rocks have strong REE signatures of aqueous high-temperature fluids. Additionally, it is also suggested that the TE1,3 can be considered as an exploration vector for different types of granite-related ore systems, especially when plotted against P2O5 (wt%). This combining geochemical features allow to divide the magmatic-hydrothermal systems in three different trends: (i) Li-Sn, Li-phosphates-bearing granite-related ore systems; (ii) W-Sn-Li, fluorapatite- and lepidolite-bearing granite-related ore systems; and (iii) Sn-Nb-Ta topaz-, tourmaline- and garnet-bearing granite-related ore systems.

## 6. Conclusions

The comprehensive multi-elemental whole-rock geochemical characterization of the main plutons and late aplite-pegmatite dykes exposed across the Segura-Panasqueira Sn-W-Li belt (Central-Iberian Zone) show that the Cambrian-Ordovician and Carboniferous-Permian granite suites: (i) display different degrees of differentiation and met-al-enrichment, and (ii) their compositional features compare well with data published for similar rocks from other Variscan segments. Increasing TE1,3 values (up to 1.4) co-vary with magmatic differentiation and metal-enrichment, and the Carboniferous-Permian granites are more differentiated, and metal specialized. The Li-Sn ore systems, Li-phosphate-bearing, Argemela RMG and aplite-pegmatite dykes from Segura deviate from this geochemical trend, displaying TE1,3 values <1.1, but also high P2O5 contents. It is then suggested that TE1,3 values and P2O5 (wt%) contents can be used together to separate three different magmatic-hydrothermal systems: (i) dominated by P+F±B (P>B), with strong aqueous high-temperature REE signatures, and related to Li-Sn Peraluminous-High-Phosphorous granites and Li-phosphates-bearing aplite-pegmatite dykes (TE1,3 <1.1); (ii) dominated by F+P±B (F>P) and related to W-Sn-Li High-Phosphorous granites and lepidolite-bearing aplite-pegmatite dykes (TE1,3 up to 1.4); and (iii) dominated by F+B±P (F>B) and related to Sn-Ta-Nb Peraluminous-Low-Phosphorous granites (TE1,3 up to 2.1). Such data suggests also that the degree of the lanthanide tetrad effect can be a very useful whole-rock geochemical fingerprint of granite differentiation and exploration vector for different types of granite-related ore systems.

Supplementary Materials: The following supporting information can be downloaded at: www.mdpi.com/xxx/s1, Figure S1: title; Table S1: title.

Author Contributions: I.M., fieldwork, geological mapping, sampling and sample preparation, conceptualization, numerical handling of analytical data, data interpretation and writing (original draft preparation, review, and editing); A.M., fieldwork, geological mapping, sampling, conceptualization, numerical handling of analytical data, data interpretation, writing (review and editing) and funding acquisition; M.C., sampling, data interpretation, writing (review and editing) and funding acquisition; M.C.B., sampling, data interpretation, writing (review and editing) and funding acquisition; I.R.C., data interpretation, writing (review and editing) and fund-ing acquisition; I.D.S., fieldwork, geological mapping, sampling, writing (review and editing) and funding acquisition; M.G., writing (review and editing) and funding acquisition. All authors have read and agreed to the published version of the manuscript.

Funding: This work was supported by Fundação para a Ciência e Tecnologia, I.P./MCTES through national funds (PID-DAC) – UIDB/50019/2020 and PD/BD/142783/2018, being also a contribution of MOSTMEG project (ERA-MIN/0002/2019), //mostmeg.rd.ciencias.ulisboa.pt/.

Acknowledgments: The authors are thankful to Beralt Tin and Wolfram S.A. for permitting the access to SCB2 drill-core from the Panasqueira Mine area. The administrative support of Célia Lee is also warmly acknowledged.
Conflicts of Interest: The authors declare no conflicts of competing financial interests or person-al relationships that could have influenced the work reported in this paper.

1. Linnen, R.L.; Van Lichtervelde, M.; Cerny, P. Granitic pegmatites as sources of strategic metals. Elements 2012, 8, 275–280.
2. Gunn, G. Critical Metals Handbook; JohnWiley & Sons, Ltd.: Hoboken, NJ, USA, 2013.
3. Dehainea, Q.; Filippova, L.O.; Glass, H.J.; Rollinson, G. Rare-metal granites as a potencial source of critical metals: A geometallurgical case study. Ore Geol. Rev. 2019, 104, 384–402.
4. Ballouard, C.; Massuyeau, M.; Elburg, M.A.; Tappe, S.; Viljoen, F.; Brandenburg, J. The magmatic and magmatic-hydrothermal evolution of felsic igneous rocks as seen through Nb-Ta geochemical fractionation, with implications for the origins of rare-metal mineralizations. Earth Sci. Rev. 2020, 203, 103115.
5. Cerný, P.; Blevin, P.L.; Cuney, M.; London, D. Granite-related ore deposits. In Economic Geology; Hedenquist, J.W., Thompson, J.F.H., Goldfarb, R.J., Richards, J.R., Eds.; Society of Economic Geologists, Inc.: Littleton, CO, USA, 2005; Volume 100th Anniversary, pp. 337–370.
6. Sami, M.; Ntaflos, T.; Farahat, E.S.; Mohamed, H.A.; Ahmed, A.F.; Hauzenberger, C. Mineralogical, geochemical and Sr-Nd isotopes characteristics of fluorite-bearing granites in the Northern Arabian-Nubian Shield, Egypt: Constraints on petrogenesis and evolution of their associated rare metal mineralization. Ore Geol. Rev. 2017, 88, 1–22.
7. Schuiling, R.D. Tin belts on the continents around the Atlantic Ocean. Econ. Geol. 1967, 62, 540–550.
8. Derré, C. Caracteristiques de la distribution des gisements à etain et tungstene dans l'ouest de l'Europe. Miner. Depos. 1982, 17, 55–77.
9. Marignac, C.; Cuney, M. Ore deposits of the French Massif Central: Insight into the metallogenesis of the Variscan collision belt. Miner. Depos. 1999, 34, 472–504.
10. Blundell, D.; Arndt, N.; Cobbold, P.R.; Heinrich, C. Geodynamics and ore deposit evolution in Europe. Ore Geol. Rev. 2005, 27, 345.
11. De Vos,W.; Batista, M.J.; Demetriades, A.; Duris, M.; Lexa, J.; Lis, J.; Marsina, K.; O'Connor, P.J. Metallogenic mineral provinces and world class ore deposits in Europe. In IUSGS/IAGC Global Geochemical Baselines; EuroGeoSurveys: Brussels, Belgium, 2005.
12. Kerrich, R.; Goldfarb, R.J.; Richards, J.P. Metallogenic provinces in an evolving geodynamic framework. In Economic Geology; Hedenquist, J.W., Thompson, J.F.H., Goldfarb, R.J., Richards, J.R., Eds.; Society of Economic Geologists, Inc.: Littleton, CO, USA, 2005; Volume 100th Anniversary, pp. 1097–1136.
13. Romer, R.L.; Thomas, R.; Stein, H.J.; Rhede, D. Dating multiply overprinted Sn-mineralized granites–examples from the Erzgebirge, Germany. Miner. Depos. 2007, 42, 337–359.
14. Harlaux, M.; Romer, R.L.; Mercadier, J.; Morloti, C.; Marignac, C.; Cuney, M. 40 Ma of hydrothermal W mineralization during the Variscan orogenic evolution of the French Massif Central revealed by U-Pb dating of wolframite. Miner. Depos. 2018, 53, 21–51.
15. Gourcerol, B.; Gloaguen, E.; Melleton, J.; Tudur, J.; Galiegue, X. Re-assessing the European lithium resource potential—A review of hard-rock resources and metallogeny. Ore Geol. Rev. 2019, 109, 494–519.
16. Bau, M. Controls on the fractionation of isovalent trace elements in magmatic and aqueous systems: Evidence from Y/Ho, Zr/Hf, and lanthanide tetrad effect. Contrib. Mineral. Petrol. 1996, 123, 323–333.
17. Bau, M. The lanthanide tetrad effect in highly evolved felsic igneous rocks—A reply to the comment by Y. Pan. Contrib. Mineral. Petrol. 1997, 128, 409–412.
18. Irber, W. The lanthanide tetrad effect and its correlation with K/Rb, Eu/Eu*, Sr/Eu, Y/Ho, and Zr/Hf of evolving peraluminous granite suites. Geochim. Cosmochim. Acta 1999, 63, 489–508.
19. Ballouard, C.; Poujol, M.; Boulvais, P.; Branquet, Y.; Tartèse, R.; Vigneresse, J.L. Nb-Ta fractionation in peraluminous granites: A marker of the magmatic-hydrothermal transition. Geology 2016, 44, 231–234.
20. Romer, R.L.; Pichavant, M. Rare metal (Sn,W, Ta-Nb, Li) granites and pegmatites. In Encyclopedia of Geology, 2nd ed.; Alderton, D., Elias, S.A., Eds.; Academic Press: Cambridge, MA, USA, 2020; pp. 840–846.

21. Masuda, A.; Kawakami, O.; Dohmoto, Y.; Takenaka, T. Lanthanide tetrad effects in nature: Two mutually opposite types W and M. Geochem. J. 1987, 21, 119–124.
22. Masuda, A.; Ikeuchi, Y. Lanthanide tetrad effect observed in marine environments. Geochem. J. 1978, 13, 19–22.
23. Masuda, A.; Akagi, T. Lanthanide tetrad effect observed in leucogranites from China. Geochem. J. 1990, 23, 245–253.
24. Akagi, T.; Nakai, S.; Shimiuzu, H.; Masuda, A. Constraints on the geochemical stage causing tetrad effect in kimuraite: Comparative studies on kimuraite and its related rocks, from REE pattern and Nd isotope ratio. Geochem. J. 1996, 30, 139–144.
25. Yang, W.; Niu, H.; Shan, Q.; Sun, W. Geochemistry of magmatic and hydrothermal zircon from the highly evolved Baerzhe alkaline granite: Implications for Zr–REE–Nb mineralization. Miner. Depos. 2014, 49, 451–470.
26. Badanina, E.V.; Sitnikova, M.A.; Gordienko, V.V.; Melcher, F.; Gäbler, H.E.; Lodziak, J.; Syritso, L.F. Mineral chemistry of columbite-tantalite from spodumene pegmatites of Kolmozero, Kola Peninsula (Russia). Ore Geol. Rev. 2015, 64, 720–735.
27. Peretyazhako, I.S.; Savina, E.A. Tetrad effects in the rare earth element patterns of granitoid rocks as an indicator of fluoride-silicate liquid immiscibility in magmatic systems. Petrology 2010, 18, 514–543.
28. Monecke, T.; Kempe, U.; Monecke, J.; Sala, M.; Wolf, D. Tetrad effect in rare earth element distribution patterns: A method of quantification with application to rock and mineral samples from granite-related rare metal deposits. Geochim. Cosmochim. Acta 2002, 66, 1185–1196.
29. Monecke, T.; Dulski, P.; Kempe, U. Origin of convex tetrads in rare earth element patterns of hydrothermally altered siliceous igneous rocks from the Zinnwald Sn–W deposit, Germany. Geochim. Cosmochim. Acta 2007, 71, 335–353.
30. Pan, Y.M. Controls on the fractionation of isovalent trace elements in magmatic and aqueous systems: Evidence from Y/Ho, Zr/Hf, and lanthanide tetrad effect—A discussion of the article by M. Bau (1996). Contrib. Mineral. Petrol. 1997, 128, 405–408.
31. Pan, Y.M.; Breaks, F.W. Rare-earth elements in fluorapatite, Separation Lake area, Ontario; evidence for S-type granite-rare-element pegmatite linkage. Can. Mineral. 1997, 35, 659–671.
32. Ribeiro, A.; Iglesias, M.; Ribeiro, M.; Pereira, E. Modéle géodynamique des Hercynides Ibériques. Comun. Serv. Geol. Port. 1983, 64, 191–214.
33. Ribeiro, A.; Quesada, C.; Dallmeyer, R. Geodynamic evolution of the Iberian Massif. In Pre-Mesozoic Geology of Iberia; Springer: Berlin, Germany, 1990; pp. 399–409.
34. Ribeiro, A.; Munhá, J.; Dias, R.; Mateus, A.; Pereira, E.; Ribeiro, M.L.; Fonseca, P.; Araújo, A.; Oliveira, J.T.; Romão, J.; et al. Geodynamic evolution of the SW Europe Variscides. Tectonics 2007, 26.
35. Martínez Catalán, J.R.; Rubio Pascual, F.J.; Díez Montes, A.; Díez Fernández, R.; Gómez Barreiro, J.; Dias da Silva, Í.; González Clavijo, E.; Ayarza, P.; Alcock, J.E. The late Variscan HT/LP metamorphic event in NW and Central Iberia: Relationships to crustal thickening, extension, orocline development and crustal evolution. Lond. Geol. Soc. 2014, 405, 225–247.
36. Dias, R.; Ribeiro, A.; Romão, J.; Coke, C.; Moreira, N. A review of the arcuate structures in the Iberian Variscides; constraints and genetic models. Tectonophysics 2016, 681, 170–194.
37. Ribeiro, A. Contribuition à l'étude tectonique de Trás-os-Montes Oriental. Comun. Serv. Geol. Port. 1974, 24, 1–168.
38. Noronha, F.; Ramos, J.; Rebelo, J.; Ribeiro, A.; Ribeiro, M. Essai de corrélation des phases de déformation hercynienne dans le Nord-Ouest Péninsulaire. Bol. Soc. Geol. Port. 1979, 21, 227–237.
39. Dias, R.; Ribeiro, A. The Ibero-Armorican Arc: A collision effect against an irregular continent? Tectonophysics 1995, 246, 113–128.
40. Azevedo, M.; Aguado, B. Origem e instalação de granitóides variscos na Zona Centro-Ibérica. In Geologia de Portugal. Geologia Pré-Mesozoica de Portugal; Escolar Editora: Lisbon, Portugal, 2013; Volume 1, pp. 377–401.
41. Azor, A.; Dias da Silva, Í.; Gómez Barreiro, J.; González-Clavijo, E.; Martínez Catalán, J.R.; Simancas, J.F.; Martínez Poyatos, D.; Pérez-Cáceres, I.; González Lodeiro, F.; Expósito, I.; et al. Deformation and Structure. In The Geology of Iberia: A Geodynamic Approach, Volume 2, The Variscan Cycle; Regional Geology Reviews; Springer: Gewerbestrasse, Switzerland, 2019; Volume 1, pp. 307–348.

42. Dallmeyer, R.D.; Martínez-Catalán, J.R.; Arenas, R.; Gil-Ibarguchi, J.I.; Gutiérrez-Alonso, G.; Farias, P.; Bastida, F. Diachronous Variscan tectonothermal activity in the NW Iberian Massif; evidence from 40Ar/39Ar dating of regional fabrics. Tectonophysics 1997, 277, 307–337.
43. Díez Fernández, R.; Pereira, M.F. Extensional orogenic collapse captured by strike-slip tectonics: Constraints from structural geology and U-Pb geochronology of the Pinhel shear zone (Variscan orogen, Iberian Massif). Tectonophysics 2016, 691, 290–310.
44. Pereira, M.F.; Díez Fernández, R.; Gama, C.; Hofmann, M.; Gärtner, A.; Linnemann, U. S-type granite generation and emplacement during a regional switch from extensional to contractional deformation (Central Iberian Zone, Iberian autochthonous domain, Variscan Orogeny). Int. J. Earth Sci. 2018, 107, 251–267.
45. Noronha, F.; Ribeiro, M.; Almeida, A.; Dória, A.; Guedes, A.; Lima, A.; Martins, H.; Sant'Ovaia, H.; Nogueira, P.; Martins, T.; et al. Jazigos filonianos hidrotermais e aplitopegmatíticos espacialmente associados a granitos (Norte de Portugal). In Geologia de Portugal: Geologia Pré-Mesozoica de Portugal; Escolar Editora: Lisbon, Portugal, 2013; Volume 1, pp. 403–438.
46. Ribeiro, A.; Antunes, M.T.; Ferreira, M.P.; Rocha, R.B.; Soares, A.F.; Zbyszewski, G.; Almeida, F.M.; Carvalho, D.; Monteiro, J.H. Introduction à la Géologie Générale du Portugal. Serv. Geol. Port. 1979, 1–114.
47. Dias da Silva, Í.; González Clavijo, E.; Díez-Montes, A. The collapse of the Variscan belt: A Variscan lateral extrusion thin-skinned structure in NW Iberia. Int. Geol. Rev. 2021, 63, 659–695.
48. Mateus, A.; Figueiras, J.; Martins, I.; Rodrigues, P.C.; Pinto, F. Relative Abundance and Compositional Variation of Silicates, Oxides and Phosphates in theW-Sn-Rich Lodes of the Panasqueira Mine (Portugal): Implications for the Ore-Forming Process. Minerals 2020, 10, 551.
49. Iglesias, M.; Ribeiro, A. Zones de cisaillement ductile dans l'arc Ibero-Armorican. Serv. Geol. Port. 1981, 67, 85–87.
50. González Clavijo, E.; Díez Balda, M.A.; Álvarez, F. Structural study of a semiductile strike-slip system in the Central Iberian Zone (Variscan Fold Belt, Spain): Structural controls on gold deposits. Geol. Runds. 1993, 82, 448–460.
51. Pereira, E.; Ribeiro, A.; Meireles, C. Cisalhamentos hercínicos e controlo de mineralizações de Sn-W, Au e U na zona centro-Ibérica em Portugal. Cuad. Lab. Xeol. Laxe Coruña 1993, 18, 89–119.
52. Valle Aguado, B.; Martínez Catalán, J.R.; Azevedo, M.R. Structure of the western termination of the Juzbado-Penalva do Castelo Shear Zone (Western Iberian Massif). In Variscan-Appalachian Dynamics: The Building of the Upper Paleozoic basement; Program and Abstracts; Basement Tectonics: A Coruña, Spain, 2000; Volume 15, pp. 287–291.
53. Gutiérrez-Alonso, G.; Collins, A.S.; Fernández-Suárez, J.; Pastor-Galán, D.; González-Clavijo, E.; Jourdan, F.; Weil, A.B.; Johnston, S.T. Dating of lithospheric buckling: 40Ar/39Ar ages of syn-orocline strike–slip shear zones in northwestern Iberia. Tectonophysics 2015, 643, 44–54.
54. Pastor-Galán, D.; Dias da Silva, Í.; Groenewegen, T.; Krijgsman,W. Tangled up in folds: Tectonic significance of superimposed folding at the core of the Central Iberian curve (West Iberia). Int. Geol. Rev. 2019, 61, 240–255.
55. Iglésias, M.; Choukroune, P. Shear zones in the Iberian Arc. J. Struct. Geol. 1980, 2, 63–68.
56. Ferreira, N.; Iglesias, M.; Noronha, F.; Pereira, E.; Ribeiro, A.; Ribeiro, M.L. Granitóides da Zona Centro Ibérica e seu enquadramento geodinâmico. In Geologia de Los Granitoides y Rocas Associadas del Macizo Hespérico Libro Homenaje a LC Garcia de Figuerola;
Bea, F., Carnicero, E., Gonzalo, J.C., Plaza, M.L., Rodríguez, M.D., Eds.; Rueda: Madrid, Spain, 1987; pp. 37–53.
57. Dias, G.T.; Leterrier, J.; Mendes, A.; Simões, P.P.; Bertrand, J.M. U-Pb zircon and monazite geochronology of post-collisional Hercynian granitoids from the Central Iberian Zone (Northern Portugal). Lithos 1998, 45, 349–369.
58. Dias, G.; Simões, P.; Ferreira, N.; Leterrier, J. Mantle and crustal sources in the genesis of late-Hercynian granitoids (NW Portugal): Geochemical and Sr-Nd isotopic constraints. Gond. Res. 2002, 5, 287–305.
59. Almeida, A.; Martins, H.; Noronha, F. Hercynian acid magmatism and related mineralisations in Northern Portugal. Gond. Res. 2002, 5, 423–434.

60. Valle Aguado, B.; Azevedo, M.R.; Schaltegger, U.; Martínez-Catalán, J.R.; Nolan, J. U/Pb zircon and monazite geochronology of Variscan magmatism related to synconvergence extension in Central Northern Portugal. Lithos 2005, 82, 169–184.
61. Martins, H.; Sant'Ovaia, H.; Noronha, F. Genesis and emplacement of felsic Variscan plutons within a deep crustal lineation, the Penacova-Régua-Verín fault: An integrated geophysics and geochemical study (NW Iberian Peninsula). Lithos 2009, 111, 142–155.
62. Martins, H.; Sant'Ovaia, H.; Abreu, J.; Oliveira, M.; Noronha, F. Emplacement of the Lavadores granite (NW Portugal): U/Pb and AMS results. Comptes Rendus Geosci. 2011, 343, 387–396.
63. Marques, F.O.; Mateus, A.; Tassinari, C.C. The Late-Variscan fault network in central-northern Portugal (NW Iberia): A reevaluation. Tectonophysics 2002, 359, 255–270.
64. Lagarde, J.L.; Capdevila, R.; Fourcade, S. Granites et collision continentale: L'exemple des granitoides carboniferes dans la chaine hercynienne ouesteuropéenne. Bull. Soc. Géol. 1992, 163, 597–610.
65. Escuder Viruete, J. Hornblende-bearing leucosome development during syn-orogenic crustal extension in the Tormes Gneiss Dome, NW Iberian Massif, Spain. Lithos 1999, 46, 751–772.
66. López-Plaza, M.; Peinado, M.; López-Moro, F.J.; Rodríguez Alonso, M.D.; Carnicero, A.; Franco, P.; Gonzalo, J.C. Contrasting mantle sources and processes involved in a peri-Gondwanan terrane: A case study of pre-Variscan mafic intrusives from the autochthon of the Central Iberian Zone. Geol. Soc. Am.-Spec. Pap. 2007, 423, 297–313.
67. Fernández-Suárez, J.; Gutierrez-Alonso, G.; Johnston, S.T.; Jeffries, T.E.; Pastor-Galán, D.; Jenner, G.A.; Murphy, J.B. Iberian late-Variscan granitoids: Some considerations on crustal sources and the significance of "mantle extraction ages". Lithos 2011, 123, 121–132.
68. López-Moro, F.J.; López-Plaza, M.; Gutiérrez-Alonso, G.; Fernández-Suárez, J.; López-Carmona, A.; Hofmann, M.; Romer, R.L. Crustal melting and recycling: Geochronology and sources of Variscan syn-kinematic anatectic granitoids of the Tormes Dome (Central Iberian Zone). A U–Pb LA-ICP-MS study. Int. J. Earth Sci. 2017, 107, 985–1004.
69. Arthaud, F.; Matte, P. Les décrochements Tardi-Hercyniens du Sud-ouest de l'Europe. Géometrie et essai de reconstitution des conditions de la déformation. Tectonophysics 1975, 25, 139–171.
70. Sousa, M. Considerações sobre a estratigrafia do Complexo Xisto-Grauváquico (CXG) e a sua relação com o Paleozóico Inferior. Quad. Geol. Ibérica 1984, 9, 9–36.
71. Pereira, E. Estudo Geológico–Estrutural da Região de Celorico de Basto e a Sua Interpretação Geodinâmica. Ph.D. Thesis, University of Lisbon, Lisbon, Portugal, 1987; p. 274.
72. Sousa, M.; Sequeira, A. Carta Geológica de Portugal à escala 1/50.000, Folha 10-D–Alijó. Serv. Geol. Port. 1987, 50.
73. Meireles, C. New data on the lithostratigraphy of beiras Group (Schist Greywacke complex) in the region of Góis-Arganil- Pampilhosa da Serra (Central Portugal). Cad. Lab. Xeolóxico Laxe 2013, 37, 105–124.
74. Silva, A. A Litostratigrafia e Estrutura do Supergrupo Dúrico-Beirão (Complexo Xisto-Grauváquico), em Portugal, e sua correlação com as correspondentes sucessões em Espanha. Bolet. Minas 2013, 48, 97–142.
75. San José, M.A.; Pieren, A.P.; García-Hidalgo, J.F.; Vilas, L.; Herranz, P.; Pelaez, J.R.; Perejon, A. Ante-Ordovician Stratigraphy. In Pre-Mesozoic Geology of Iberia; Dallmeyer, R.D., Martínez García, E., Eds.; Springer: Berlin, Germany, 1990; pp. 147–159.
76. Valladares, M.I.; Barba, P.; Ugidos, J.M.; Colmenero, J.R.; Armenteros, I. Upper Neoproterozoic–Lower Cambrian sedimentary successions in the Central Iberian Zone (Spain): Sequence stratigraphy, petrology and chemostratigraphy. Implications for other European zones. Int. J. Earth Sci. 2000, 89, 2–20.
77. Ugidos, J.M.; Barba, P.; Valladares, M.I. Chapter Four—Review of the Upper Ediacaran-Lower Cambrian detrital series in Central and North Iberia: NE Africa as possible source area. In Stratigraphy & Timescales; Montenari, M., Ed.; Academic Press: Cambridge, MA, USA, 2020; Volume 5, pp. 147–268.
78. Castro, A.; Patiño Douce, A.E.; Corretgé, L.G.; De La Rosa, J.D.; El-Biad, M.; El-Hmidi, H. Origin of peraluminous granites and granodiorites, Iberian massif, Spain: An experimental test of granite petrogenesis. Contrib. Mineral. Petrol. 1999, 135, 255–276.
79. Villaseca, C.; Downes, H.; Pin, C.; Barbero, L. Nature and Composition of the Lower Continental Crust in Central Spain and the Granulite-Granite Linkage: Inferences from Granulitic Xenoliths. J. Petrol. 1999, 40, 1465–1496.

80. Ribeiro, M.; Castro, A.; Almeida, A.; González Menéndez, L.; Jesus, A.; Lains, J.A.; Lopes, J.C.; Martins, H.C.B.; Mata, J.; Mateus, A.; et al. Variscan Magmatism. In The Geology of Iberia: A Geodynamic Approach, Volume 2, The Variscan Cycle; Regional Geology Reviews; Springer: Gewerbestrasse, Switzerland, 2019; Volume 1, pp. 497–526.
81. Pinto, M.S.; Casquet, C.; Ibarrola, E.; Corretgé, L.S.; Ferreira, M.P. Síntese geocronológica dos granitóides do Maciço Hespérico. In Geologia de los Granitoides y Rocas Associadas del Macizo Hespérico Libro Homenaje a L.C. Garcia de Figuerola; Bea, F., Carnicero, E., Gonzalo, J.C., López Plaza, M., Rodríguez, M.D., Eds.; Rueda: Madrid, Spain, 1987; pp. 69–86.
82. Dias, G.T. Fontes de granitóides hercínicos da Zona Centro-Ibérica (Norte de Portugal): Evidências isotópicas (Sr, Nd). In Geoquímica e Petrogénese de Rochas Granitóides; Neiva, A.M.R., Ed.; Academia das Ciências de Lisboa: Lisboa, Portugal, 2001; pp. 21–43.
83. Azevedo, M.; Aguado, B. Origem e instalação de granitóides variscos na Zona Centro Ibérica. In Geologia de Portugal no contexto da Ibéria; Dias, R., Araújo, A., Terrinha, P., Kulberg, C., Eds.; University Évora: Évora, Portugal, 2006; pp. 107–121.
84. Mateus, A.; Noronha, F. Sistemas mineralizantes epigenéticos na Zona Centro-Ibérica; expressão da estruturação orogénica Meso-a Tardi-Varisca. In Ciências Geológicas: Ensino e Investigação e sua História; Cotelo Neiva, J.M., Ribeiro, A., Mendes Victor, L., Noronha, F., Ramalho, M., Eds.; Associação Portuguesa de Geólogos and Sociedade Geológica de Portugal, Lisboa: Lisbon, Portugal, 2010; Volume II, pp. 47–61.
85. Inverno, C.; Ribeiro, M.L. Fracturação e cortejo filoniano nas Minas da Argemela (Fundão). Comun. Serv. Geol. Port. 1980, 66, 185–193.
86. Ribeiro, A.; Pereira, E. Controles paleogeográficos, petrológicos e estruturais na génese dos jazigos portugueses de estanho e volfrâmio. Geonovas 1982, 1, 23–31.
87. Derré, C.; Lécolle, M.; Roger, G.; Carvalho, J. Tectonics, magmatism, hydrothermalism and sets of flat joints locally filled by Sn-W aplite-pegmatite and quartz veins; southeastern border of the Serra da Estrela granitic massif (Beira Baixa, Portugal). Ore Geol. Rev. 1986, 1, 43–56.
88. Ribeiro, M.L. Modelos de implantação dos granitos variscos portugueses. In Geoquímica e Petrogénese de Rochas Granitóides; Neiva, A.M.R., Ed.; Academia das Ciências de Lisboa: Lisboa, Portugal, 2001; pp. 33–52.
89. Cathelineau, M.; Boiron, M.C.; Marignac, C.; Dour, M.; Dejean, M.; Carocci, E.; Truche, L.; Pinto, F. High pressure and temperatures during the early stages of tungsten deposition at Panasqueira revealed by fluid inclusions in topaz. Ore Geol. Rev. 2020,
126, 103741.
90. Noronha, F. Estudo Metalogénico da Área Tunstífera da Borralha. Ph.D. Thesis, University Porto, Porto, Portugal, 1983; p. 413.
91. Noronha, F.; Vindel, E.; López, J.A.; Dória, A.; Garcia, E.; Boiron, M.-C.; Cathelineau, M. Fluids related to tungsten ore deposits in Northern Portugal and Spanish Central System: A comparative study. Rev. Soc. Geol. España 1999, 12, 397–403.
92. Conde, L.; Pereira, V.; Ribeiro, A.; Thadeu, D. Jazigos Hipogénicos de Estanho e volfrâmio. In I Congresso Hispano-Luso-Americano de Geologia Económica; Direção Geral de Minas e Serviços Geológicos: Lisboa, Portugal, 1979; p. 81.
93. Thadeu, D. Características da mineralização hipogénica estano-volframítica portuguesa. Bol. Ord. Eng. 1965, 10, 61–81.
94. Clark, A.H. Preliminary of the temperatures and confining pressures of granite emplacement and mineralization, Panasqueira, Portugal. Trans. Inst. Min. Metall. 1964, 73, 813–824.
Minerals 2022, 12, 1067 26 of 27
95. Portugal Ferreira, M.; Costa, V.; Regêncio Macedo, C.A.; Gama Pereira, L. Datações K-Ar em biotite das rochas granitóides da Cova da Beira (Portugal Central). Mem. Not. Publ. Mus. Lab. Mineral. Geol. 1977, 84, 39–48.
96. Kelly, W.C.; Reye, R.O. Geologic, fluid inclusion, and stable isotope studies of the tin-tungsten deposits of Panasqueira, Portugal. Econ. Geol. 1979, 74, 1721–1882.
97. Bussink, R.W. Geochemistry of the Panasqueira tungsten-tin deposit, Portugal. Geol. Ultraiect. 1984, 33, 1–159.
98. Priem, D.; Tex, T. Tracing crustal evolution in the NW Iberian Peninsula through the Rb-Sr and U-Pb systematics of Paleozoic granitoids: A review. Phys. Earth Planet. Inter. 1984, 35, 121–130.

99. Pereira, A.; Pereira, L.; Macedo, C. Os plutonitos da zebreira (Castelo Branco): Idade e enquadramento estructural. Mem. Not. Publ. Mus. Lab. Mineral. Geol. 1986, 101, 21–31.
100. Antunes, I.M.; Neiva, A.M.; Silva, M.M.; Corfu, F. Geochemistry of S-type granitic rocks from the reversely zoned Castelo Branco pluton (central Portugal). Lithos 2008, 103, 445–465.
101. Antunes, I.M.; Neiva, A.M.; Silva, M.M.; Corfu, F. The genesis of I- and S-type granitoid rocks of the Early Ordovician Oledo pluton, Central Iberian Zone (central Portugal). Lithos 2009, 111, 168–185.
102. Antunes, I.M.; Neiva, A.M.; Corfu, F. New emplacement age to the Fundão pluton (central Portugal): U-Pb isotopic data. In Proceedings of the European Mineralogical Conference, Frankfurt, Germany, 2–6 September 2012.
103. Antunes, I.M.; Neiva, A.M.; Ramos, J.M.; Silva, P.B.; Silva, M.M.; Corfu, F. Petrogenetic links between lepidolite-subtype aplite-pegmatite, aplite veins and associated granites at Segura (central Portugal). Geochemistry 2013, 73, 323–341.
104. Antunes, I.M. Características geoquímicas e geocronológicas do plutão de Fundão—Implicações geotectónicas. In Proceedings of the XII Congresso Ibérico de Geoquímica, Évora, Portugal, 22–26 September 2019; pp. 133–136.
105. Martins Peres, A.; Caraça Valente, A.J.; Lucas Gonçalves, J. Carta Geológica de Portugal à escala 1/50.000, Folha 21-B—Quadrasais. Serv. Geol. Port. 1960.
106. Avila Martins, J.; Cândido de Medeiros, A.; Peres, A.; Pilar, L.; Pinto Mesquita, L. Carta Geológica de Portugal à escala 1/50.000, Folha 21-A- Sabugal. Serv. Geol. Port. 1964.
107. Ribeiro, O.; Ribeiro Ferreira, C. Carta Geológica de Portugal à escala 1/50.000, Folha 24-D—Castelo Branco. Serv. Geol. Port. 1966.
108. Perdigão, J.C.; Moreira, P.A. Carta Geológica de Portugal à escala 1/50.000, Folha 21-D—Vale Feitoso. Serv. Geol. Port. 1975.
109. Teixeira, C.; de Carvalho, H.; Paula Santos, J. Carta Geológica de Portugal à escala 1/50.000, Folha 20-B—Covilhã. Serv. Geol. Port. 1975.
110. Oliveira, J.T.; Pereira, E.; Ramalho, M.; Antunes, M.T.; Monteiro, J.H. Carta Geológica de Portugal à escala 1/500.000. Serv. Geol. Port. 1992.
111. Sequeira, A.; Proença Cunha, P.; Ribeiro, M. Carta Geológica de Portugal à escala 1/50.000, Folha 25-B—Salvaterra do Extremo. Inst. Geol. Min. 1999.
112. Romão, J.; Ferreira da Silva, A.; Proença Cunha, P.; Pereira, A. Carta Geológica de Portugal à escala 1/50.000, Folhas 25-C, 25-D e
29-A—Rosmaninhal, Segura e Retorta. Lab. Geol. Min. 2010.
113. Gonçalves, A.; Sant'Ovaia, H.; Noronha, F. Geochemical Signature and Magnetic Fabric of Capinha Massif (Fundão, Central Portugal): Genesis, Emplacement and Relation with W–Sn Mineralizations. Minerals 2020, 10, 557.
114. Neiva, A.M.; Costa Campos, T. Genesis of the zoned granitic pluton of Penamacor-Monsanto, Central Portugal. Mem. Not. Publ. Mus. Lab. Mineral. Geol. 1992, 114, 51–68.
115. Ribeiro da Costa, I.; Antunes, I.M.; Mourão, C.; Recio, C.; Guimarães, F.; Ramos, J.F.; Barriga, F.J.A.S. Contact metamorphism associated to the Penamacor-Monsanto granitic intrusion (Central Portugal): Geochemical, isotopic and mineralogical features. J. Iber. Geol. 2018, 44, 335–353.
116. Michaud, J.A.S.; Pichavant, M. Magmatic fractionation and the magmatic-hydrothermal transition in rare metal granites: Evidence from Argemela (Central Portugal). Geochim. Cosmochim. Acta 2020, 289, 130–157.
117. Marignac, C.; Cuney, M.; Cathelineau, M.; Lecomte, A.; Carocci, E.; Pinto, F. The Panasqueira Rare Metal Granite Suites and Their Involvement in the Genesis of theWorld-Class PanasqueiraW–Sn–Cu Vein Deposit: A Petrographic, Mineralogical, and Geochemical Study. Minerals 2020, 10, 562.
118. Debon, F.; Lefort, P. A cationic classification of common plutonic rocks and their magmatic associations: Principles, method, applications. Bul. Min. 1988, 111, 493–510.
119. Shand, S.J. Eruptive Rocks. Their Genesis Composition. Classification, and Their Relation to Ore-Deposits with a Chapter on Meteorite; John Wiley & Sons, Ltd.: Hoboken, NJ, USA, 1943.
120. Frost, B.R.; Barnes, C.G.; Collins, W.J.; Argulus, R.J.; Ellis, D.J.; Frost, C.D. A geochemical classification for granitic rocks. J. Petrol.2001, 42, 2033–2048.
121. Frost, B.R.; Frost, C.D. A geochemical classification for feldspathic igneous rocks. J. Petrol. 2008, 49, 1955–1969.

122. El Bouseily, A.; El Sokkary, A. The relation between Rb, Ba, and Sr in granitic rocks. Geochem. Geol. 1975, 16, 207–219.
123. Pearce, J.A.; Harris, N.B.W.; Tindle, A.G. Trace element discrimination diagrams for the tectonic interpretation of granitic rocks. J. Petrol. 1984, 25, 956–983.
124. Cuney, M. Felsic magmatism and uranium deposits. Bull. Soc. Géol. France 2014, 185, 75–92.
125. Rudnick, R.L.; Gao, S. Composition of the continental crust. Treat. Geoch. 2014, 4, 1–51.
126. McDonough,W.F.; Sun, S.S. The composition of the Earth. Chem. Geol. 1995, 120, 223–253.
127. Yuan, S.D.;Williams-Jones, A.E.; Mao, J.W.; Zhao, P.L.; Yan, C.; Zhang, D.L. The origin of the Zhangjianlong tungsten deposit, South China: Implications for W-Sn mineralization in large granite batholiths. Econ. Geol. 2018, 113, 1193–1208.
128. Castro, A.; Pereira,M.F.; Rodríguez, C.; Fernández, C.; de la Rosa, J.D. Atypical peri-Gondwanan granodiorite-tonalite magmatism from Southern Iberia. Origin of magmas and implications. Lithos 2020, 372–373, 1–14.
129. López-Moro, F.J.; Polonio, F.G.; González, T.L.; Contreras, J.L.S.; Fernández, A.F.; Benito, M.C.M. Ta and Sn concentration by muscovite fractionation and degassing in a lens-like granite body: The case study of the Penouta rare-metal albite granite (NWSpain). Ore Geol. Rev. 2017, 82, 10–30.
130. Roda-Robles, E.; Villaseca, C.; Pesquera, A.; Gil-Crespo, P.P.; Vieira, R.; Lima, A.; Garate-Olave, I. Petrogenetic relationships between Variscan granitoids and Li-(F-P)-rich aplite-pegmatites in the Central Iberian Zone: Geological and geochemical constraints and implications for other regions from the European Variscides. Ore Geol. Rev. 2018, 95, 408–430.
131. Audétat, A.; Günther, D.; Heinrich, C.A. Magmatic-hydrothermal evolution in a fractionating granite: A microchemical study of the Sn-WF-mineralized Mole Granite (Australia). Geoch. Cosm Acta 2000, 64, 3373–3393.
132. Simons, B.; Andersen, J.C.; Shail, R.K.; Jenner, F.E. Fractionation of Li, Be, Ga, Nb, Ta, In, Sn, Sb,Wand Bi in the peraluminous early permian Variscan granites of the Cornubian Batholith: Precursor processes to magmatic-hydrothermal mineralisation. Lithos 2017, 278, 491–512.
133. Michaud, J.A.S.; Gumiaux, C.; Pichavant, M.; Gloaguen, E.; Marcoux, E. From magmatic to hydrothermal Sn-Li-(Nb-Ta-W) mineralization: The Argemela area (central Portugal). Ore Geol. Rev. 2020, 116, 103215.
134. Zhao, P.L.; Zajacz, Z.; Tsay, A.; Yuan, S.D. Magmatic-hydrothermal tin deposits form in response to efficient tin extraction upon magma degassing. Geochim. Cosmoch. Acta 2022, 316, 331–346.

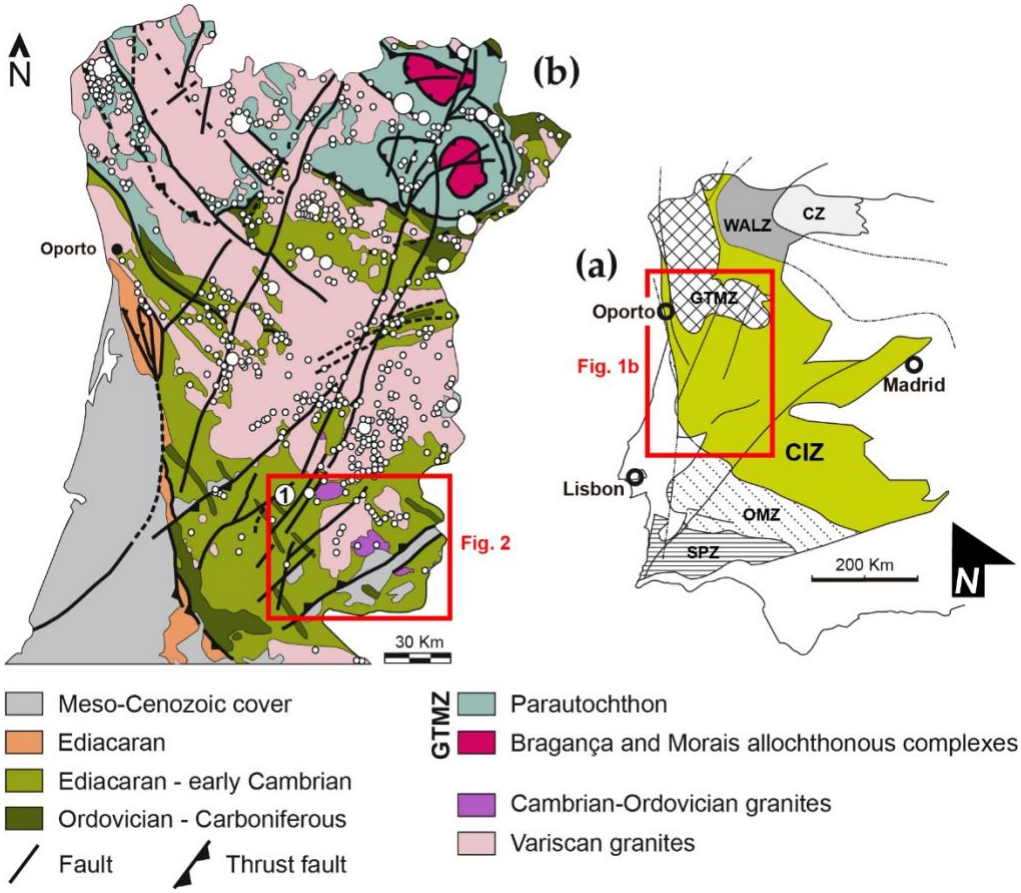


Figure 1. (a) Geotectonic map of the Iberian Massif [adapted from 42]. CZ - Cantabrian Zone; WALZ – West Asturian-Leonese Zone; GTMZ - Galicia Trás-os-Montes Zone; CIZ - Central Ibe-rian Zone; OMZ - Ossa Morena Zone; SPZ - South Portuguese Zone. (b) Simplified geological map of central and northern Portugal [adapted from “Carta Geológica de Portugal 1:1 000 000”, Geo-logical Survey of Portugal, LNEG, 2010; modified from 43]. The white circles represent the main known tungsten and tin deposits (mineral deposits location taken from the official national cata-logue SIORMINP – LNEG). 1 – Panasqueira Mine.

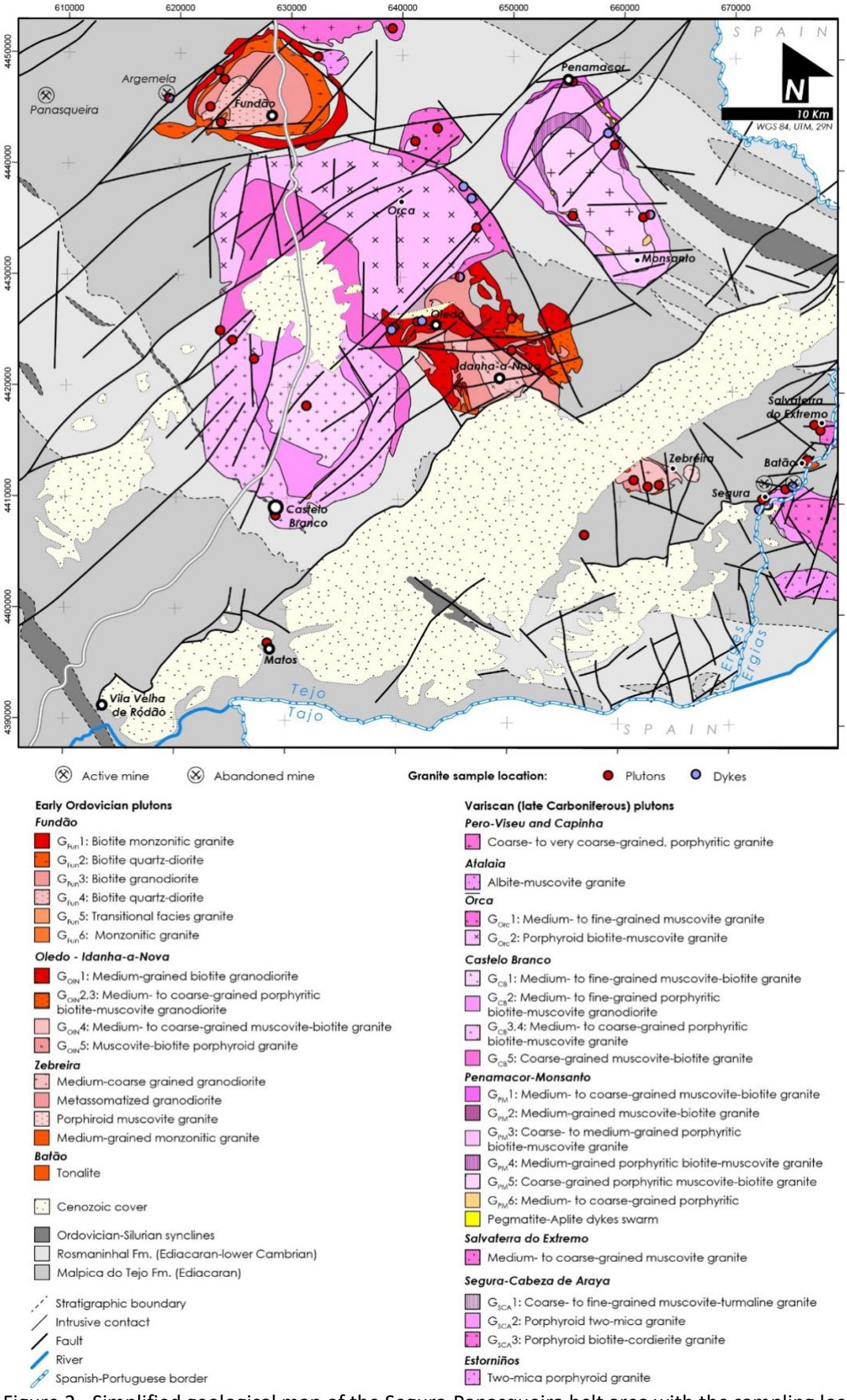


Figure 2 - Simplified geological map of the Segura-Panasqueira belt area with the sampling location. The map includes recent field appraisals along with outputs from a harmonized database built on a long series of previous works [61,86-93].

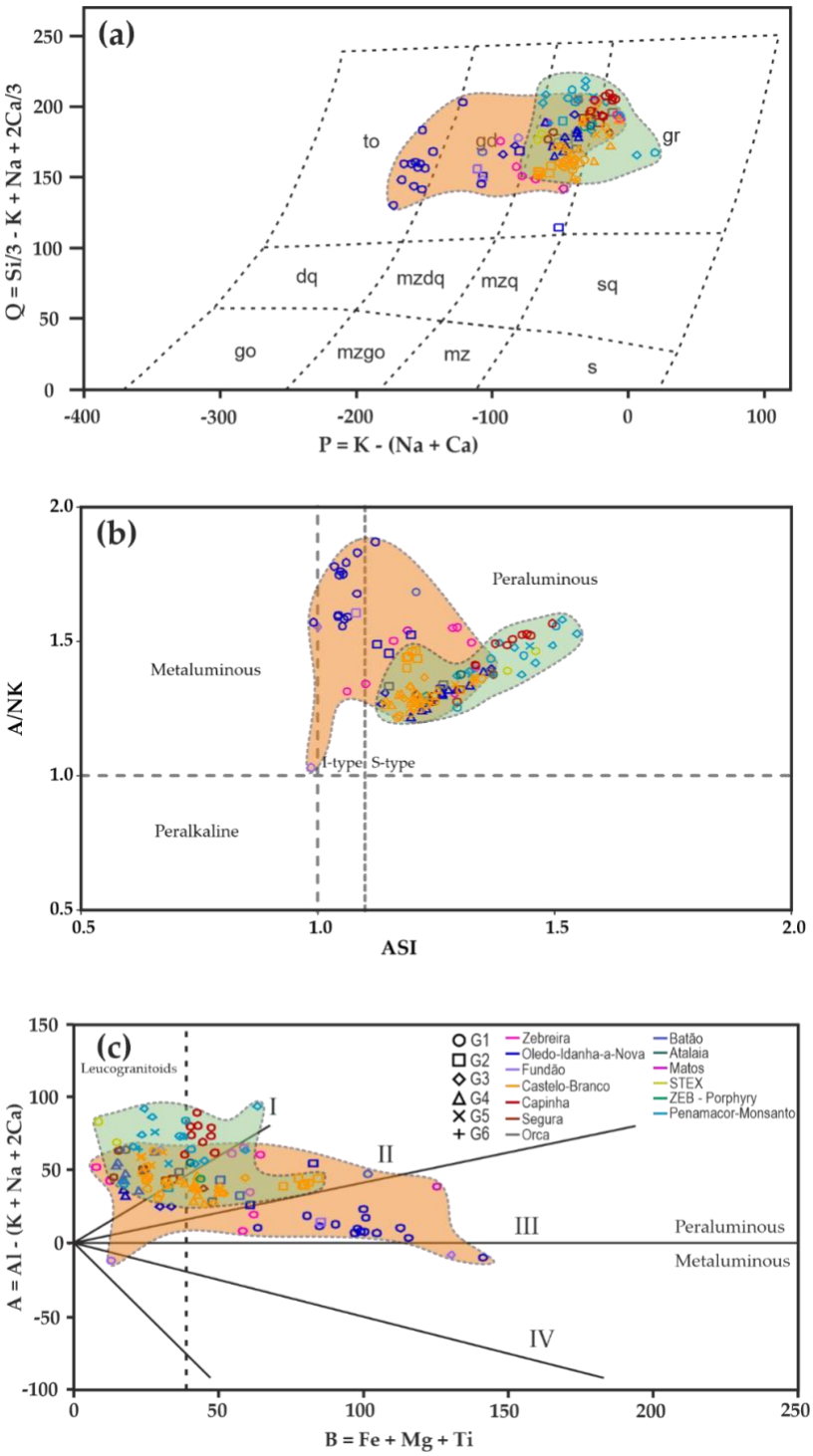


Figure 3 – Classification diagrams for the Cambrian-Ordovician (orange compositional field) and Variscan (green compositional field) granite suites. (a) Q-P diagram [adapted from 99]. ad – adamellite; dq – quartz diorite; gd – granodiorite; go – gabbro, diorite, anorthosite; gr – granite; mz – monzonite, mzdq – quartz monzodiorite, quartz monzogabbro; mzgo – monzogabbro, monzodiorite; mzq – quartz monzonite; s – syenite; sq – quartz syenite; to – tonalite, trondhjemite; (b) ASI vs. A/NK diagram [adapted from 100,101]; (c) A-B diagram [adapted from 99]. Sectors I, II, III – peraluminous rocks with muscovite > biotite, biotite > muscovite and biotite, respectively; Sector IV – metaluminous rocks with biotite + amphibole ± pyroxene. Symbols and colors in (c).

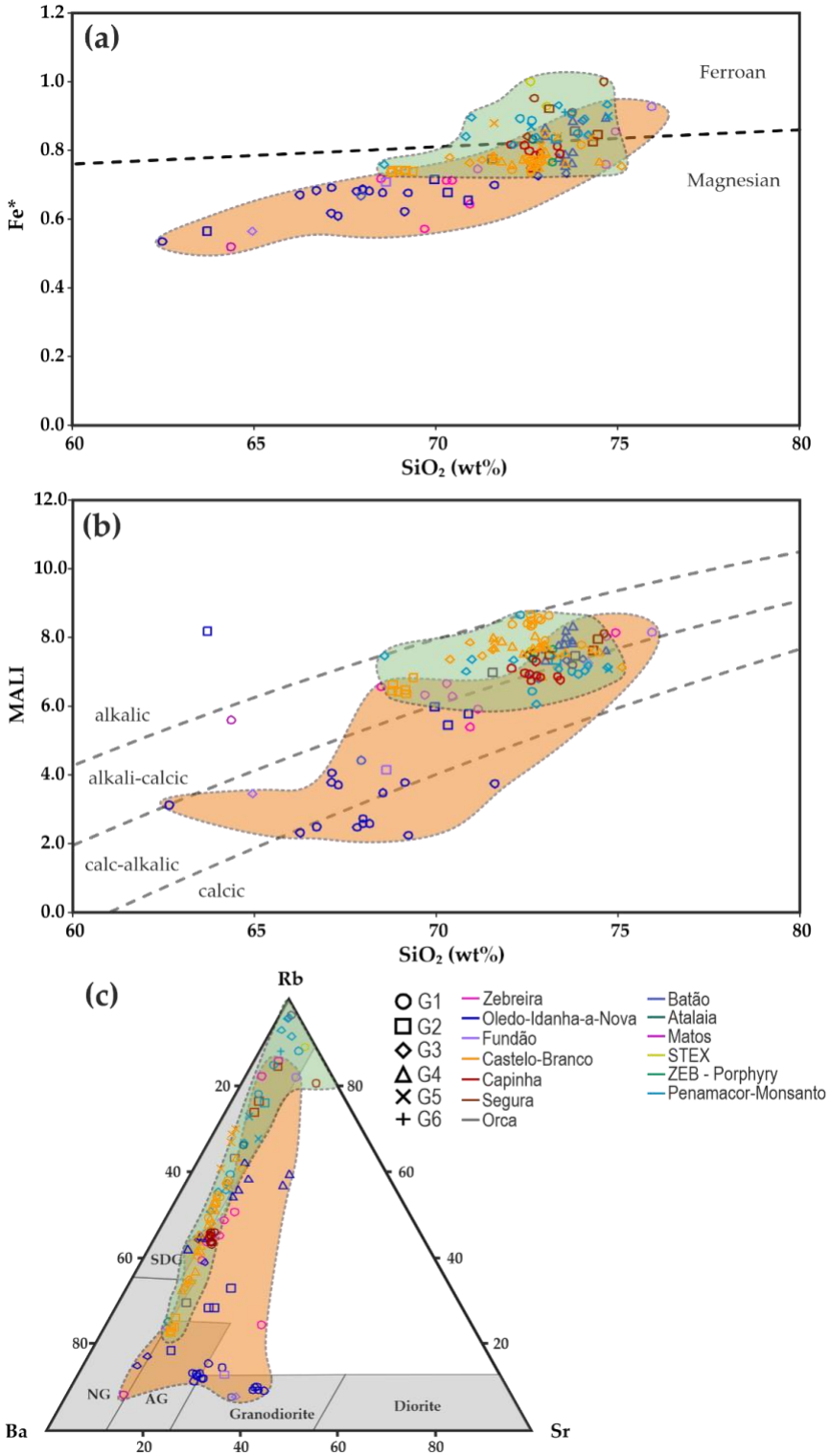


Figure 4 – Classification diagrams for the Cambrian-Ordovician (orange compositional field) and Variscan (green compositional field) granite suites. (a) SiO2 vs. Fe* diagram [adapted from 102]; (b) SiO2 (wt%) vs. MALI diagram [adapted from 102]; (c) Ba-Rb-Sr ternary diagram [adapted from 103]. AG – Anomalous Granites; NG – Normal Granites; SDG – Strongly Differentiated Granites.

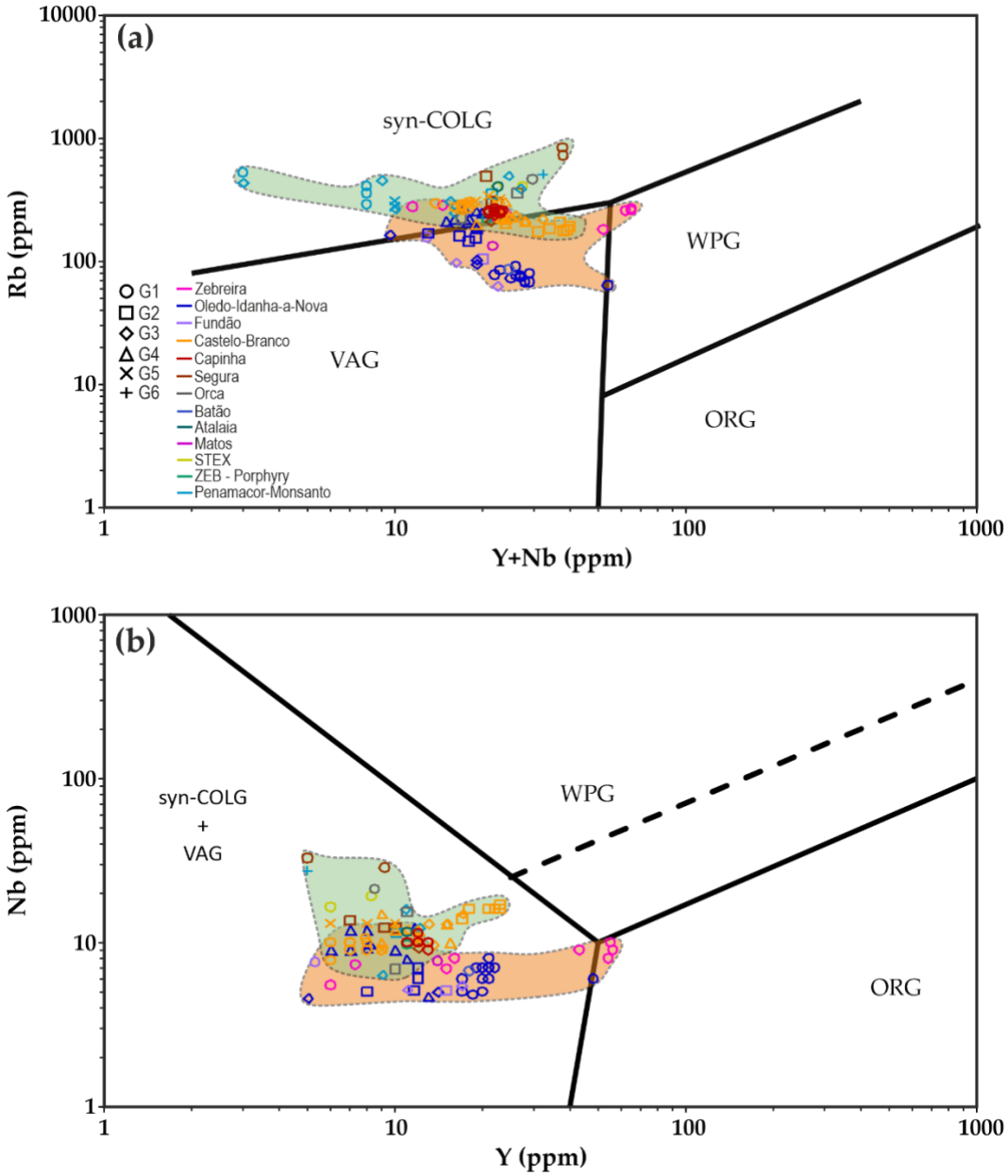


Figure 5 - Tectonic discrimination diagrams for the Cambrian-Ordovician (orange composition-al field) and Variscan (green compositional field) granite suites [adapted from 96]. VAG – Volcanic Arc Granites; syn-COLG – syn-Collisional Granites; WPG – Within-Plate Granites; ORG – Ocean-Ridge Granites. Symbols and colors in (a).

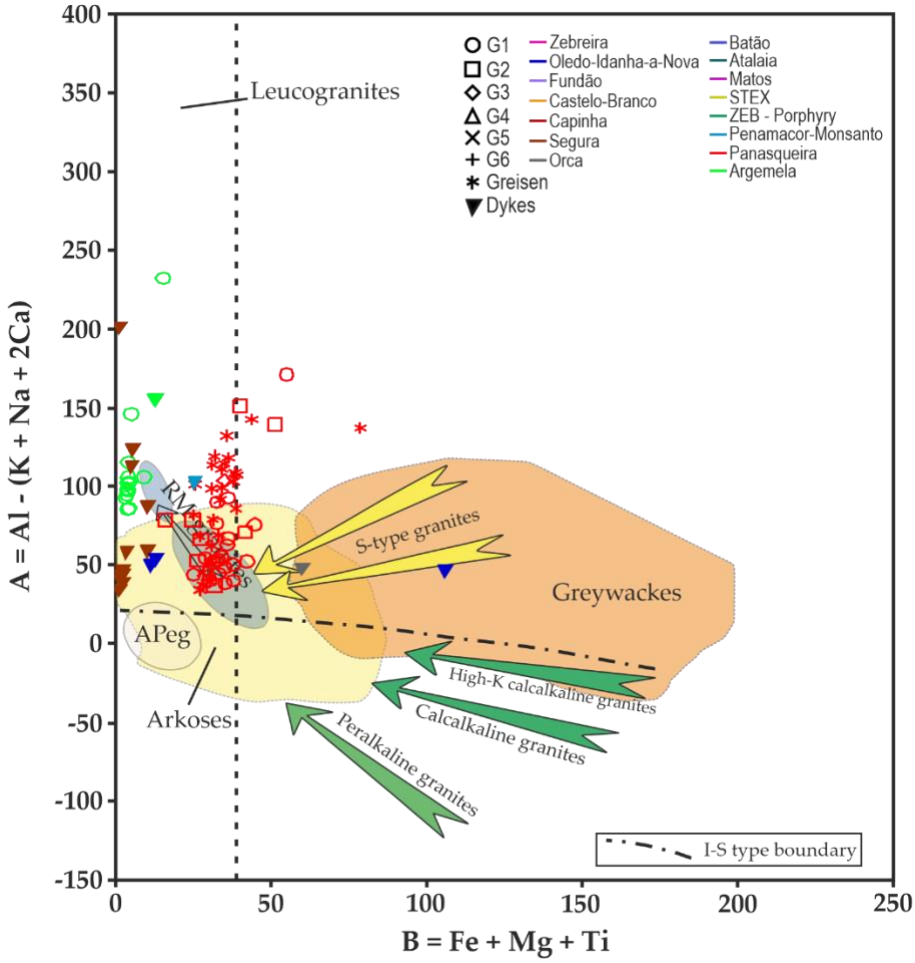


Figure 6 – Modified A-B classification diagram for the highly differentiated granite facies and aplite-pegmatites dykes from Oledo-Idanha-a-Nova, Orca, Penamacor-Monsanto, Segura, Panasqueira and Argemela [adapted from 19, 105].

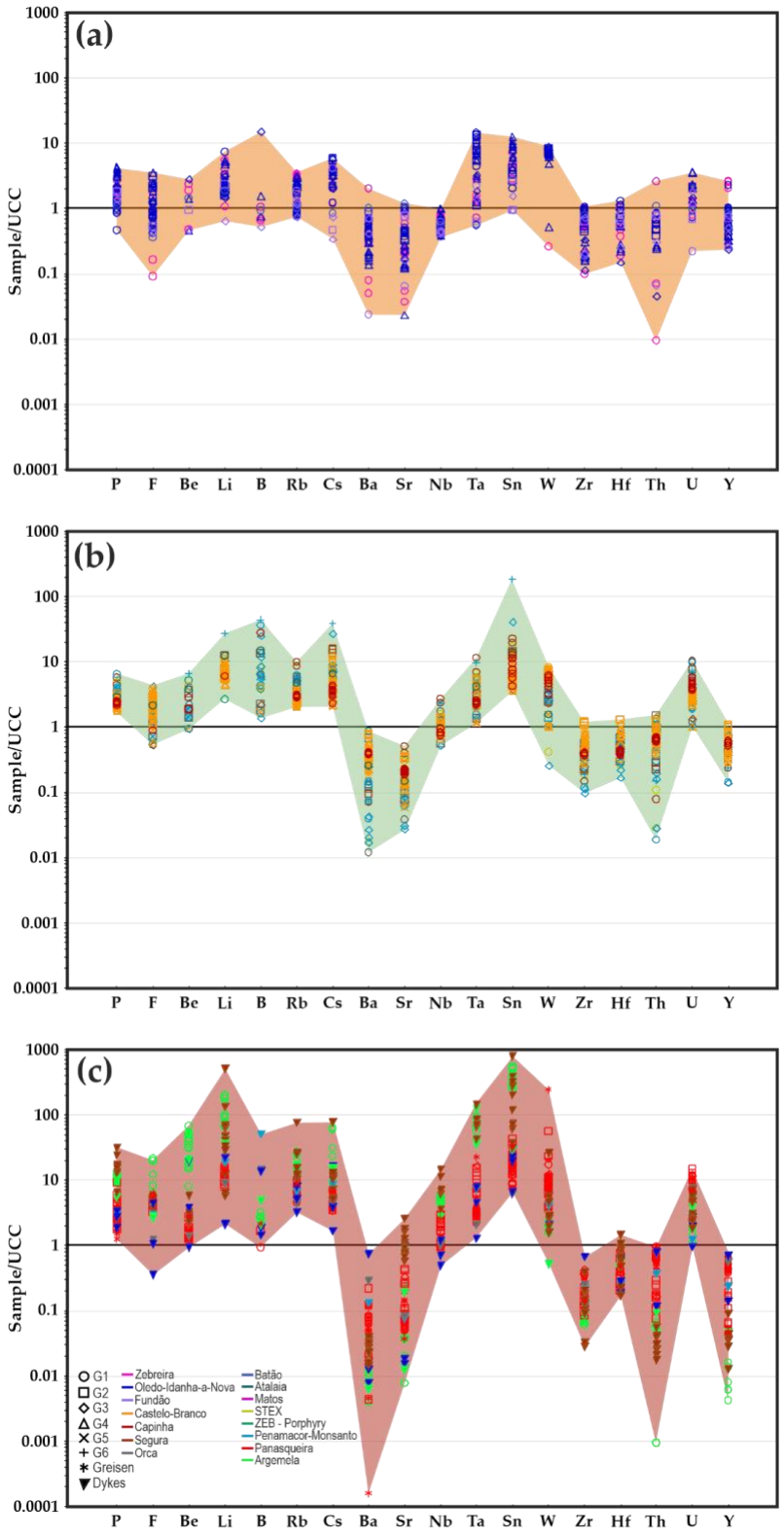


Figure 7 - Upper Continental Crust-normalized multi-element concentration patterns for the (a) Cambrian-Ordovician (orange compositional field); (b) Variscan (green compositional field); and (c) highly differentiated granite facies and aplite-pegmatite dykes (pink compositional field). Upper Continental Crust (UCC) normalization values after Rudnick and Gao, 2014. Symbols and colors in (c).

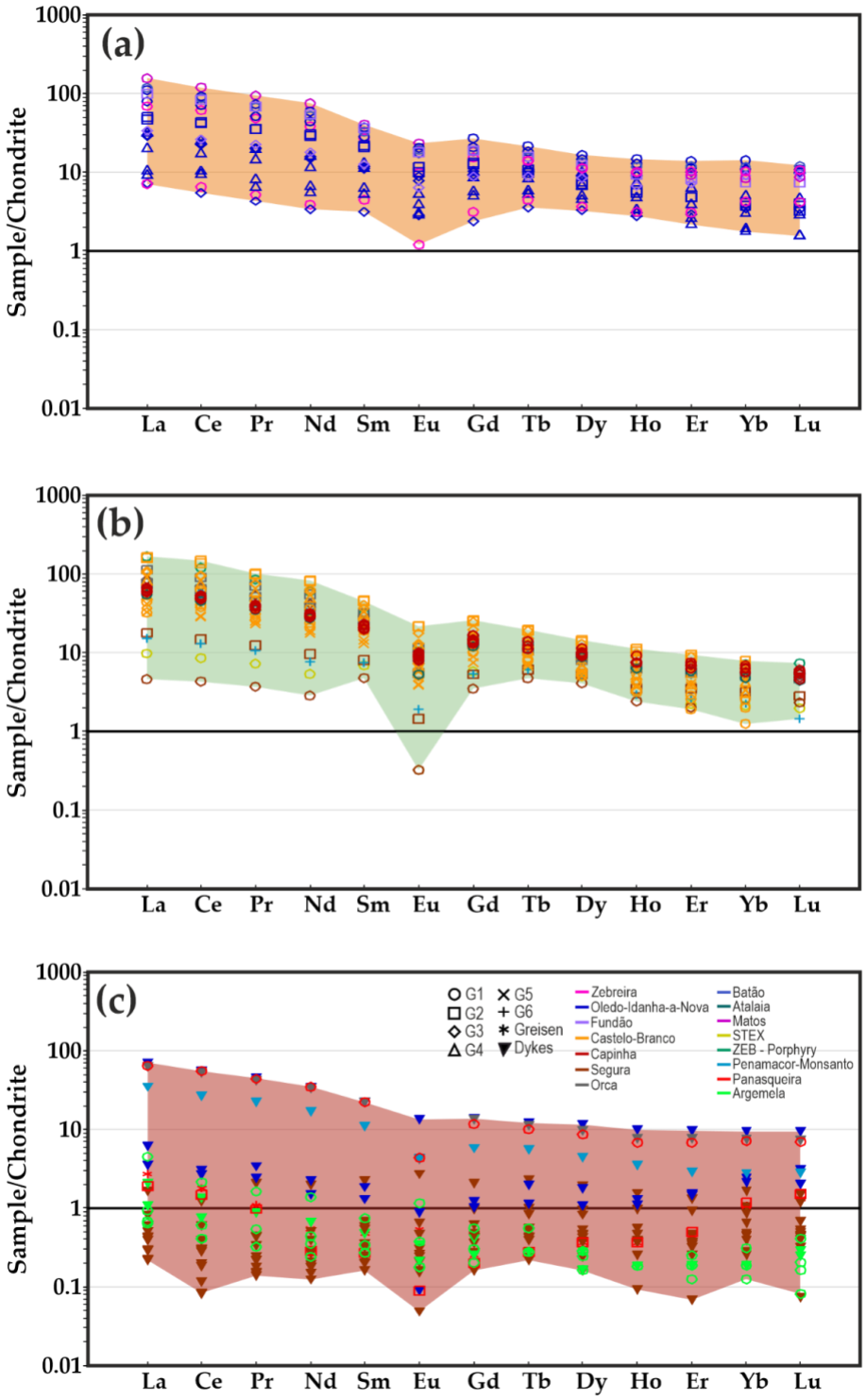


Figure 8 – REE Chondrite-normalization diagram for the (a) Cambrian-Ordovician (orange compositional field); (b) Variscan (green compositional field); and (c) highly differentiated granite facies and aplite-pegmatite dykes (red compositional field). Chondrite normalization values after McDonough and Sun, 1995. Symbols and colors in (c).

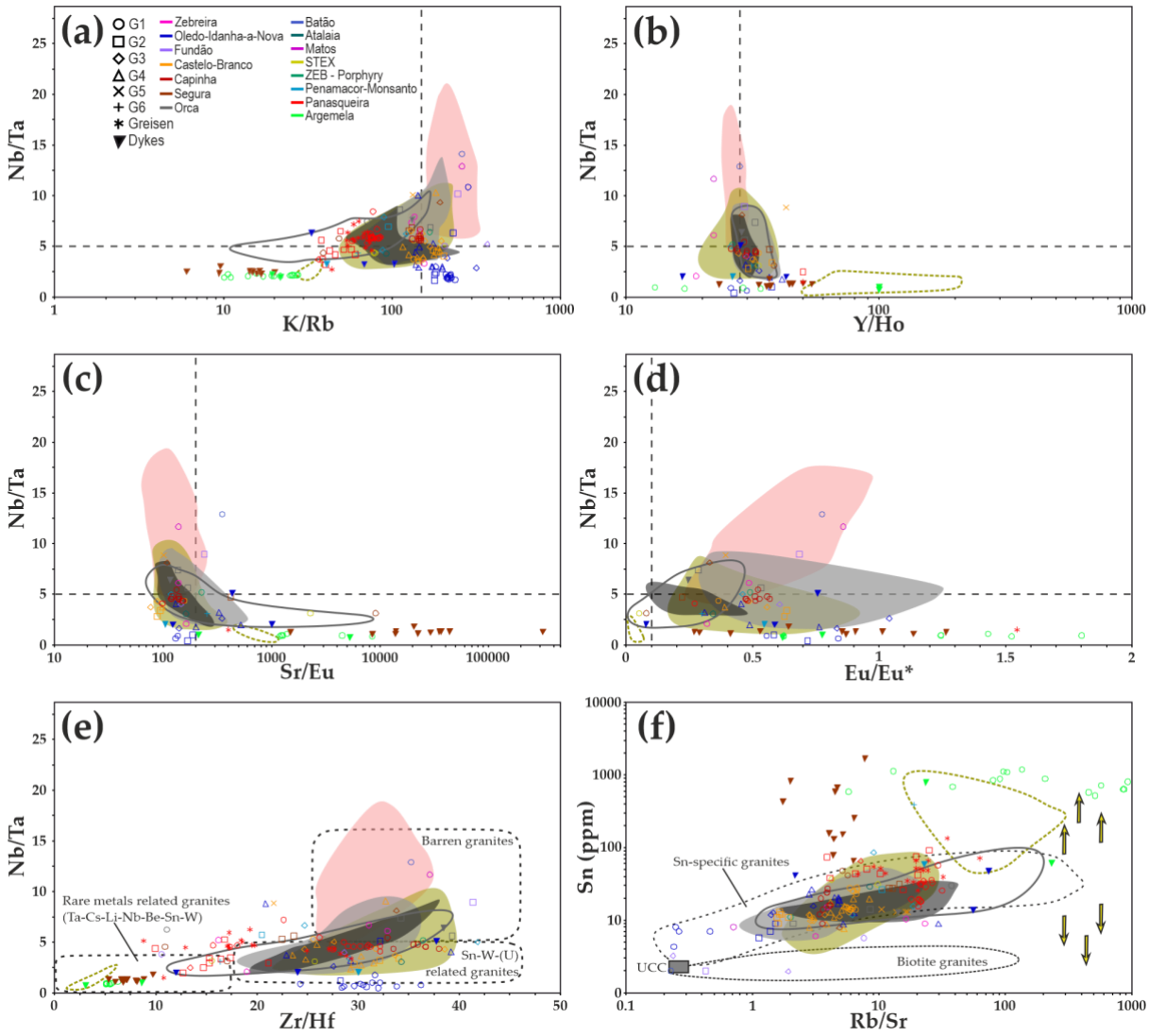


Figure 9 – Trace element ratios variation diagrams for granite facies exposed in the SeguraPanasqueira area, evidencing different degrees of differentiation, late-stage magmatic-hydrothermal interactions and metal specialization. (a) K/Rb vs. Nb/Ta; (b) Y/Ho vs. Nb/Ta; (c) Sr/Eu vs. Nb/Ta; (d) Eu/Eu* vs. Nb/Ta; (e) Zr/Hf vs. Nb/Ta diagram separating barren and ore-related peraluminous granites [adapted from 18]. (f) Rb/Sr vs. Sn diagram evidencing the enrichment in Sn with the increase of the degree of differentiation [adapted from 19]. This diagram discriminates biotite granites from Sn-specialized granites, and compositional deviations related to late-stage melt-hydrothermal transition (yellow arrows). Plotted in the different diagrams are the representative compositional fields of other granite suites from: Cambrian-Ordovician Bei-ra-Extremadura batholith [pink compositional area, 108]; Armorican Massif [grey compositional area, 4 and references therein]; Iberian Massif [greenish-yellow compositional area, 4 and refer-ences therein, 110 and references therein], Erzgebirge-Fichtelgebirge [solid dark grey line, 4 and references therein]; Cornwall [black compositional area, 4 and references therein] and Penouta RMG [dashed greenish-yellow line, 4 and references therein]. The black dashed lines represent reference values of Nb/Ta <5, K/Rb <150, Y/Ho ≠28, Sr/Eu >200 and Eu/Eu* <0.1, normally dis-played by peraluminous granites that experienced significant interaction with high-temperature hydrothermal fluids [4,17]. Symbols and colors in (a).

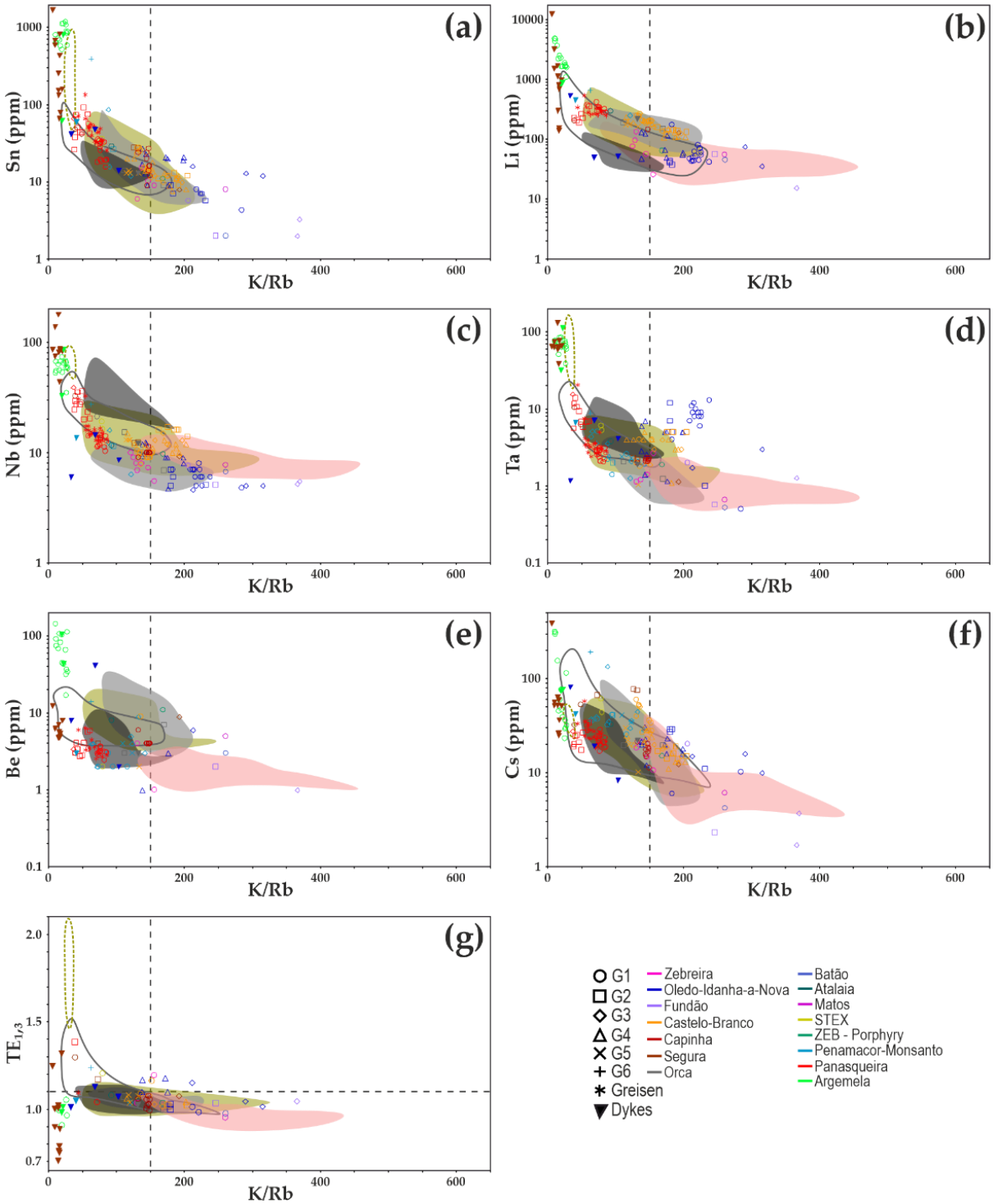


Figure 10 – (a-f) Selected trace element contents vs. K/Rb ratios for the granite facies exposed across the Segura-Panasqueira area, evidencing different degrees of differentiation (K/Rb) and enrichments in common rare-metals in granite-related ore systems (Sn, Li, Nb, Ta, Be and Cs). It should be noted that the granite rocks studied in this work present low W contents (up to 50.44 ppm), often being below the detection limits of the analytical methods used, and therefore W is not considered. (g) K/Rb vs. TE1,3, showing the correlation between granite differentiation and the degree of the tetrad effect; Representative compositional fields of other granite suites are plotted as in Figure 9. The black dashed lines represent reference values of K/Rb <150 and TE1,3 >1.1 normally displayed by peraluminous granites that experienced significant interaction with high-temperature hydrothermal fluids [4,17].

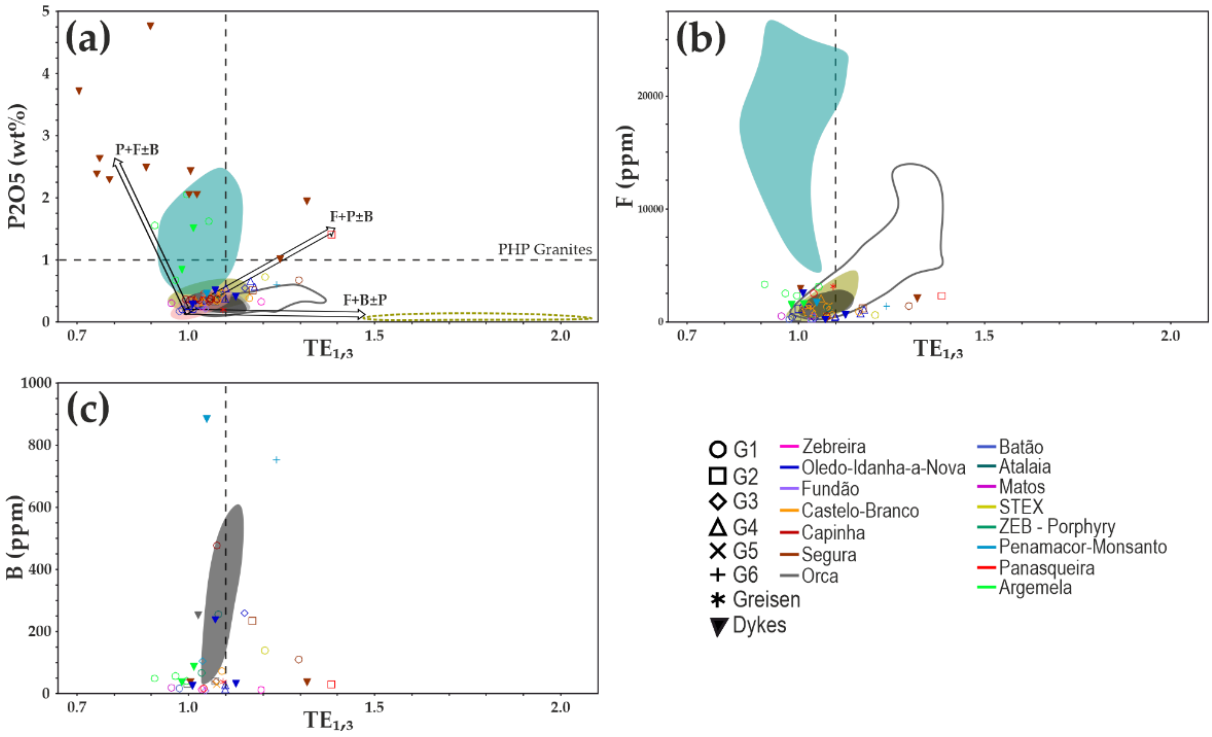


Figure 11 – Degree of the tetrad effect (TE1,3) vs. (a) P2O5 (wt%), (b) F (ppm) and (c) B (ppm), showing the influence of the increasing concentration in fluxing elements on the REE fractionation. Three main compositional trends are distinguished, representing magmatic-hydrothermal systems related to different types of mineralization: (i) Peraluminous High-Phosphorus Li-Sn magmatic-hydrothermal systems dominated by P+F±B (P>F), in which Li is mostly incorporated in phosphate mineral phases; (ii) Peraluminous High-Phosphorus W-Sn-Li magmatic-hydrothermal systems dominated by F+P±B (F>P) and variably enriched in Li-bearing micas; and (iii) Peraluminous Low-Phosphorus Sn-Nb-Ta magmatic-hydrothermal systems dominated by F+B±P (F>B). Representative compositional fields of granitoid suites are plotted: Cambrian-Ordovician Bei-ra-Extremadura batholith [pink compositional area, 108]; Armorican Massif [grey compositional area, 4 and references therein]; Iberian Massif [greenish-yellow compositional area, 4 and references therein, 110 and references therein], Erzgebirge-Fichtelgebirge [solid dark grey line, 4 and references therein]; Cornwall [black compositional area, 4 and references therein], Penouta RMG [dashed greenish-yellow line, 4 and references therein] and Beauvoir (blue compositional area). The black dashed lines represent reference values of TE1,3 >1.1 normally displayed by peraluminous granites that show effects of significant interaction with high-temperature aqueous fluids [4, 17]. Due to incomplete analytical packages, samples from Beira-Extremadura batolith, Iberian Massif, Erzgebirge-Fichtelgebirge, Cornwall and Penouta RMG are not plotted on all graphs. For the same reason, the Beauvoir data is only plotted in the graphs a) and b) of this figure.